Metal-Assisted Chemical Etching of Silicon: A Review

Zhipeng Huang, Nadine Geyer,* Peter Werner, Johannes de Boor, and Ulrich Gösele*

In memory of Prof. Ulrich Gösele

This article presents an overview of the essential aspects in the fabrication of silicon and some silicon/germanium nanostructures by metal-assisted chemical etching. First, the basic process and mechanism of metal-assisted chemical etching is introduced. Then, the various influences of the noble metal, the etchant, temperature, illumination, and intrinsic properties of the silicon substrate (e.g., orientation, doping type, doping level) are presented. The anisotropic and the isotropic etching behaviors of silicon under various conditions are presented. Template-based metal-assisted chemical etching methods are introduced, including templates based on nanosphere lithography, anodic aluminum oxide masks, interference lithography, and block-copolymer masks. The metal-assisted chemical etching of other semiconductors is also introduced. A brief introduction to the application of Si nanostructures obtained by metal-assisted chemical etching is given, demonstrating the promising potential applications of metal-assisted chemical etching. Finally, some open questions in the understanding of metal-assisted chemical etching are compiled.

1. Introduction

Nanostructures of silicon (Si), which remains the most important material for current semiconductor industry, are well-documented as promising building blocks for devices in the fields of nanoelectronics,[1,2] opto-electronics,[3] energy conversion,[4–9] and energy storage,[10,11] as well as bio- and chemical sensors.[12,13] Characteristic parameters, such as crystalline orientation,[14,15] crystalline quality,[16] strain,[15,17] orientation relative to the substrate[5] and size affect the properties of Si nanostructures[18] and are thus important for their application in devices.

Controllable fabrication of Si nanostructures is a prerequisite for their device applications. Numerous methods have been developed to fabricate Si nanostructures using top-down or bottom-up approaches, such as vapor-liquid-solid (VLS) growth, reactive ion etching (RIE), electrochemical etching, or metal-assisted chemical etching, all of which aim to control various parameters of the Si structures. Among these methods, metal-assisted chemical etching has attracted increasing attention in recent years for several reasons. First, metal-assisted chemical etching is a simple and low-cost method for fabricating various Si nanostructures with the ability to control various parameters (e.g., cross-sectional shape, diameter, length, orientation, doping type, and doping level). Almost all procedures can be accomplished in a chemical lab without expensive equipment. Second, metal-assisted chemical etching enables control of the orientation of Si nanostructures (e.g., nanowire, pore) relative to the substrate. In contrast, in VLS-based growth of Si nanowires, the crystallographic orientation of Si nanowire depends upon the diameter of nanowire.[19] Due to the existence of equivalent crystallographic directions, it is difficult to grow epitaxial Si nanowires with uniform orientation relative to the surface of the Si substrate. For example, the growth of epitaxial and vertical [110] nanowires on (110) substrates or [100] nanowires on (100) substrates has not yet been accomplished without the use of an appropriate template. On the other hand, electrochemical etching is well-known to occur anisotropically along <100> directions. In contrast, although the metal-assisted chemical etching is intrinsically anisotropic, methods have been developed to control the etching direction, enabling the fabrication of vertically aligned Si nanowire on (100) and non-(100) substrates or in certain inclined directions on non-(100) substrates.[20,21] Third, VLS-based methods can only be used to grow wires with circular cross-sections, while metal-assisted chemical etching is much more flexible and can be used to make higher surface-to-volume ratio structures.[22,23] Fourth, the crystalline quality of Si nanowires fabricated by metal-assisted etching from single crystalline substrates generally is high. Although their surfaces are typically rougher than those of nanowires obtained by VLS growth, the nanowires do not contain the obvious crystallographic defects induced by solution-based etching, while dry etching (e.g., RIE) tends to introduce defects in a region close to the etched Si surfaces.[16] Fifth, there is no obvious limitation on the size of features fabricated by metal-assisted chemical etching. The method can be utilized to fabricate straight and well-defined pores or wires with diameters as small as 5 nm or as large as 1 μm. However, there is a well-known $2W_{sc}$ rule (W_{sc} is the width of the space charge region in the Si substrate at the Si/solution interface) that limits the feature size of structure obtained from electrochemical etching, at least in the area of macroporous silicon etching.[24,25]

Dr. Z. Huang, N. Geyer, Dr. P. Werner, J. de Boor, Prof. U. Gösele
Max Planck Institute of Microstructure Physics
Weinberg 2, D-06120 Halle, Germany
E-mail: zphuang@ujs.edu.cn; ngeyer@mpi-halle.mpg.de
Dr. Z. Huang
Functional Molecular Materials Centre
Scientific Research Academy
Jiangsu University
Zhenjiang, 212013, P. R. China

DOI: 10.1002/adma.201001784

Therefore, metal-assisted chemical etching has become increasingly important in the last decade. The method has been utilized to fabricate various Si or Si/Ge nanostructures. The structures fabricated by metal-assisted chemical etching have demonstrated their application potentials in fields ranging from solar energy conversion,[4–9] thermal power conversion,[26] and energy storage,[11] to chemical and biological sensing[27,28] and biomimic superhydrophobicity.[29–31]

In this review, an overview on the fabrication of nanostructures based on metal-assisted chemical etching of Si and Si-based semiconductors is presented, including the etching process and mechanism (Section 2) and the dependence of the morphologies of the etched structures on the metal used (Section 3), the etchant (Section 4), the temperature and illumination (Section 5), and the type of Si substrate used (Section 6). Typical methods to fabricate patterned Si nanostructures are discussed in Section 7. The results from literature are summarized to give a comprehensive picture of metal-assisted chemical etching, and various etching behaviors are explained within the self-consistent picture as much as possible. Nevertheless, it is necessary to point out here that the study of the mechanism for metal-assisted chemical etching has not yet reached a real mature stage. There are still several phenomena which are presently not well-understood. The still open questions are compiled at the end of this review.

Zhipeng Huang received a B.S. and a Ph. D. in materials science and engineering from Tsinghua University, P.R. China in 2002 and 2007, respectively. He did postdoctoral research at the Max Planck Institute of Microstructure Physics in Halle, Germany from 2007–2009. He is currently professor at the Functional Molecular Materials Centre, Scientific Research Academy, Jiangsu University, P.R. China. His main research interest is the controllable fabrication of Si nanostructures and their applications.

Nadine Geyer studied physics at the Martin-Luther-University Halle-Wittenberg, Germany, where she wrote her diploma thesis in the field of metal-assisted chemical etching and graduated in 2007. After that she joined the Max Planck Institute of Microstructure Physics and began her Ph. D. under the supervision of Prof. U. Gösele. Her current research interests focus on the fabrication and characterization of silicon and silicon/germanium superlattice nanowires, as well as the investigation of the underlying metal-assisted chemical etching mechanism.

2. Methods and Mechanisms

2.1. History and Basic Phenomenon

The first demonstration of metal-assisted chemical etching of Si was reported in 1997. Porous Si was fabricated by etching an aluminum (Al) covered Si substrate in a solution composed of HF, HNO_3, and H_2O. The incubation time necessary for the formation of porous Si was dramatically decreased due to the presence of the Al film on the surface of the Si substrate.[32] The widely used metal-assisted chemical etching method was first investigated in some detail by Li and Bohn, who found that a thin layer of noble metal (e.g., Au, Pt, or Au/Pd alloy) sputtered on the surface of a Si substrate catalyzed the etching of Si in a mixed solution containing HF, H_2O_2, and EtOH, resulting in straight pores or columnar structures.[33] The etching method described by Li and Bohn gained increasing attention and various approaches derived from their method were developed to fabricate Si-based nanostructures.

In a typical metal-assisted chemical etching procedure, a Si substrate partly covered by a noble metal is subjected to an etchant composed of HF and an oxidative agent. Typically, the Si beneath the noble metal is etched much faster than the Si without noble metal coverage. As a result, the noble metal sinks into the Si substrate, generating pores in the Si substrate or, additionally, Si wires. The detailed geometries of the resulting Si structures depend mostly on the initial morphology of the noble metal coverage. Under certain conditions, microporous structures (analogous to the case found in electrochemical etching and stain etching, with pore dimensions in the range of a few nanometers) form in the regions without noble metal coverage, which will be denoted as the "off-metal area" in the rest of the article.[33] In addition, a pore induced directly by the sinking in of a noble metal particle is sometimes surrounded by a microporous structure.[34] In this section, the basic phenomena and processes in metal-assisted chemical etching are introduced.

2.2. Reactions

For simplicity, the discussion in this section is focused on the following representative case: a Si substrate in contact with an isolated noble metal particle is etched in an etchant consisting of HF and H_2O_2. The influence of noble metal morphology, etchant, and electrical properties and the crystallographic orientation of the Si substrate will be discussed in detail in the following sections. It is well-accepted that the chemical or electrochemical reactions occur preferentially near the noble metal. Various possible cathode and anode reactions[33,35–41] have been proposed to describe the metal-assisted chemical etching analogous to the anodic etching of Si in HF[42] or stain etching of Si in HF/HNO_3.[43]

It is well accepted that the H_2O_2 is reduced at the metal (cathode reaction):

$$H_2O_2 + 2H^+ \rightarrow 2H_2O + 2h^+ \quad (1)$$

Meanwhile, Li and Bohn[33] and Harade et al.[44] proposed that the reduction of protons into hydrogen was another cathode reaction in addition to reaction (1):

$$2H^+ \rightarrow H_2 \uparrow + 2h^+ \quad (2)$$

In contrast, Chartier et al.[39] attributed the gas evolution during the etching to an anode reaction. The conclusion of Chartier et al. came from the judgment that H_2O_2 instead of H^+ was the principal reaction agent at cathodic sites, because in a H_2O_2-free and O_2-free HF solution, no etching occurred in a Pt-particle-loaded Si substrate.[45] Meanwhile, the possibility that gas was generated from a decay of H_2O_2 was excluded because gas evolution did not occur on an Ag-particle-loaded Si substrate in solution with high concentration of H_2O_2 in the absence of HF.[39]

At the anode, the Si substrate is oxidized and dissolved. There are numerous models proposed for the dissolution process of Si (anode reaction), which can be catalogued into three groups: (RI) Direct dissolution of Si in tetravalent state[33,35,37,38,44,46–48]

$$Si + 4h^+ + 4HF \rightarrow SiF_4 + 4H^+ \quad (3)$$

$$SiF_4 + 2HF \rightarrow H_2SiF_6 \quad (4)$$

(RII) Direct dissolution of Si in divalent state[36,39]

$$Si + 4HF_2^- \rightarrow SiF_6^{2-} + 2HF + H_2 \uparrow + 2e^- \quad (5)$$

(RIII) Si oxide formation followed by dissolution of oxide[39,40,49–53]

$$Si + 2H_2O \rightarrow SiO_2 + 4H^+ + 4e^- \quad (6)$$

$$SiO_2 + 6HF \rightarrow H_2SiF_6 + 2H_2O \quad (7)$$

Model RII and RIII differ in whether Si oxide is formed at the surface of the Si substrate before the dissolution of Si and whether H_2 is generated accompanying the dissolution of Si. It seems that model RII happens because hydrogen is generated in a typical etching. However, whether model RIII occurs simultaneously remains an open question due to the difficulty in in situ exploration of the surface state and the uncertainty in ex situ study of the Si surface state (e.g., oxide might form during the handling of the etched structure for transmission electron microscopy (TEM) characterization). Chartier et al. proposed a mixed reaction composed of divalent and tetravalent dissolution for the dissolution of Si in metal-assisted chemical etching:[39]

$$Si + 6HF + nh^+ \rightarrow H_2SiF_6 + nH^+ + \frac{4-n}{2}H_2 \uparrow \quad (8)$$

and the overall reaction is:

$$Si + \frac{n}{2}H_2O_2 + 6HF \rightarrow nH_2O + H_2SiF_6 + \frac{4-n}{2}H_2 \uparrow \quad (9)$$

They found that the etching rate reached a maximum at $\rho \approx 80\%$, where ρ was defined as $[HF]/([HF]+[H_2O_2])$. Based on the assumption that the maximum etching rate was related to the stoichiometry of the reaction, the maximum etching rate at $\rho \approx 80\%$ suggested that n equals 3 in the above overall redox reaction.[39]

2.3. Hole Injection and Role of Metal

Charge transfer is necessary for the oxidation and dissolution of Si. Hole injection is well-documented as a charge transfer process for electroless etching of Si in HF/HNO_3 solution[43,54] and metal-assisted chemical etching of Si, despite the discrepancy in explaining the origin of gas evolution.[33,46,55–57] In this scenario, the noble metal acts as a microscopic cathode on which the reduction of the oxidant occurs (cathode reaction 1). The generated holes are then injected into the Si substrate in contact with the noble metal. Accordingly, the Si atoms under the noble metal are oxidized due to the hole injection and dissolved by HF (anode reaction 2). Many phenomena in metal-assisted chemical etching can be qualitatively explained by hole injection from the noble metal into the Si substrate and the diffusion of holes within the Si substrate, such as solution-dependent etching morphologies (Section 4) and doping-level-dependent etching morphologies (Section 5).

The electrochemical potential of H_2O_2 is much more positive than the valence band of Si and more positive than oxidants usually used in stain etching of Si (e.g., HNO_3,[43,54] $Fe(NO_3)_3$,[58,59] $KMnO_4$,[60] $KBrO_3$,[60,61] $K_2Cr_2O_7$[60], etc). From the energy point of view, H_2O_2 can inject holes into the valence band of Si (**Figure 1a**), independent of the doping type and doping level. Thus, a Si substrate subjected to HF/H_2O_2 solution should be etched. The etching of Si by HF/H_2O_2 does occur, but the etching rate is lower than 10 nm per h in an etchant with a concentration of H_2O_2 much higher than that used in metal-assisted chemical etching.[62] In practice, the presence of a noble metal is necessary for fast etching of the Si substrate in solution with certain oxidants (e.g., H_2O_2, O_2 bubble, or O_2 dissolved in the H_2O). Therefore, it is natural to attribute the preferentially observed reduction of H_2O_2 or O_2 on the surface of the metal, compared to the surface of Si, to a kinetic reason. The cathode reaction 1 occurs faster on the surface of noble metals than on a bare silicon surface. Noble metals (e.g., Pt,[63–65] Pd,[66] Au,[67] and Ag[68]) have been widely used to catalytically reduce H_2O and O_2. This might help to explain why a bare Si substrate is etched very slowly in HF/H_2O_2,[33] but very fast in a HF solution containing HNO_3, in which the reduction of HNO_3 is an autocatalytic process due to the presence of an important intermediate, HNO_2.[54]

Once the oxidant is reduced on the surface of noble metal, holes are injected into the Si substrate. Chattopadhyay et al. sketched the energy levels of Si substrate and the electrochemical potential of H_2O_2/H_2O and suggested that holes were injected deep into the valence band via Pt particles in the case of etching a Pt-loaded Si substrate with $HF/H_2O_2/H_2O$ solution (Figure 1b).[35] Similarly, to explain the etching of Si in Ag/HF solution, Peng et al. qualitatively compared the electrochemical electron energy levels of the Si band edges and the

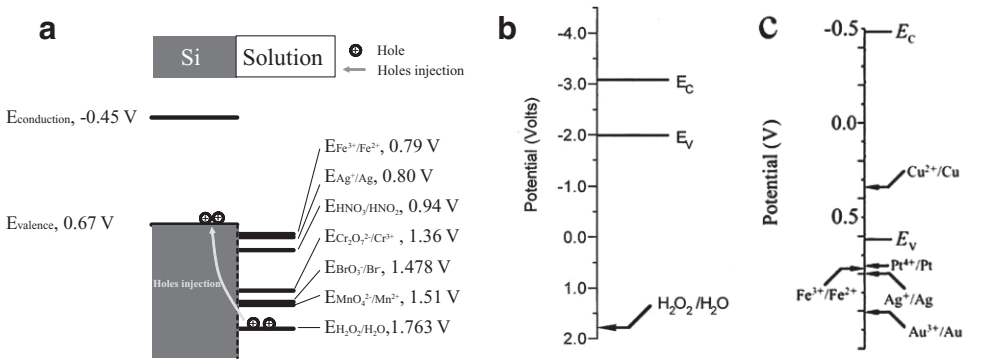

Figure 1. a) Scheme of the potential relationship between bands in a Si substrate and standard potentials of various oxidants. b) Comparison of the Si band edge energies and the H_2O_2/H_2O redox potential on the electrochemical energy scale, indicating that holes are injected deep into the valence band. Adapted with permission.[35] Copyright 2002, AIP. c) Qualitative diagram of the comparison between the electrochemical electron energy levels of the Si band edges (E_c and E_v are the conduction and valence bands, respectively) and five redox systems, $AuCl_4^-/Au$, $PtCl_6^{2-}/Pt$, Ag_+/Ag, Cu^{2+}/Cu, and Fe^{3+}/Fe^{2+}, in HF solution. Adapted with permission.[51] Copyright 2006, Wiley-VCH.

electrochemical potential of five redox systems (Figure 1c) and suggested that the reduction of Ag took place around existing Ag nuclei and Si was oxidized and dissolved.[51] The charge transfer between Si and noble metal would be heavily affected by the surface band bending of Si, which hasn't, however, been included in the models proposed by Chattopadhyay et al. and Peng et al. Meanwhile, the surface band bending of the Si substrate is determined by the doping type and doping level of the Si substrate, the surface state of Si substrate, the Fermi level and size of noble metal, and the component of the etchant. These factors have not been discussed in the etching mechanism of Si in literature. A scenario clearly depicting the energy levels in the path of charge transfer (i.e., Si substrate and noble metal) and the role of energy levels in the metal-assisted chemical etching remains lacking. Moreover, since the hole and subsequent electron transfer for oxidation of Si occurs at the surface of the Si, the surface state of Si is of importance in exploring the etching mechanism. Up to now, the surface state of Si in metal-assisted chemical etching has not been experimentally revealed or systematically discussion at the atomic scale in the literature. Therefore, the simple energy picture shown in Figure 1b,c does not contain sufficient kinetics to explain the different etching speeds of the p-type and n-type Si substrate and the different etched morphologies of lightly and highly doped Si substrates (Section 6.2).

2.4. Mass Transfer

It has been speculated that the Si atoms are oxidized and dissolved at the interface between the noble metal and the Si substrate and that the reagent and byproduct diffuses along this interface (Model I, **Figure 2**).[50,51] This assumption is plausible for the specific case in which the etching is assisted by noble metal particles with small lateral size so that the diffusion of the reagent and the byproduct along the interface between the noble metal and the Si involves only a short distance and may be easily accomplished. However, due to difficulties in observing the in situ etching process, there are no explicit experimental results that support this assumption. On the other hand, although it has not been discussed in the literature in the field of metal-assisted chemical etching, there is another possibility concerning mass transfer during the etching. That is, the Si atoms that are in contact with a noble metal are dissolved in the noble metal and then diffuse through the noble metal to the noble metal/solution interface where the silicon atoms are oxidized and etched away at the noble metal/solution interface (Model II, Figure 2). This mechanism would somehow be analogous to the well-known phenomenon that a Si substrate covered with a noble metal (film or particle) is catalytically oxidized at low temperature, or even at room temperature, in oxygen or air.[69–73] In this phenomenon, the back bonds of the Si atoms at the interface between the Si substrate and the noble metal are broken; the free Si atoms are dissolved into the noble metal, diffuse through the noble metal, and are thermally oxidized on the surface of the noble metal. If the Si is covered with a noble metal with a relatively large lateral size (e.g., larger than 1 μm), lateral diffusion of the reactant and the byproduct along the interface of Si and the noble metal (Model I) is a long distance diffusion process, while diffusion of Si atoms through the metal involves a relatively short distance (typically a few tens of

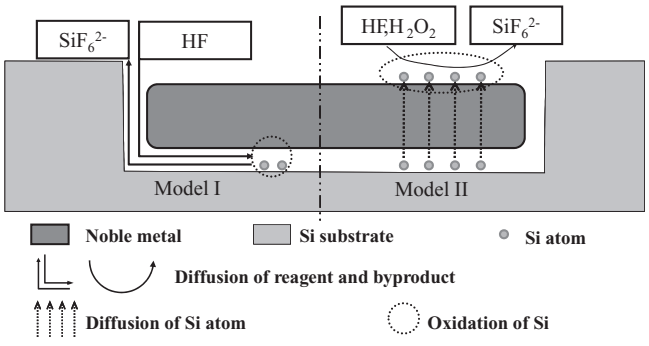

Figure 2. Scheme of two possible diffusion models during metal-assisted chemical etching. Model I: the reagent and byproduct diffuse along the interface between the noble metal and the wall of the etched structure. Model II: A Si atom is dissolved into noble metal and diffuses through noble metal and is then oxidized on the surface of noble metal.

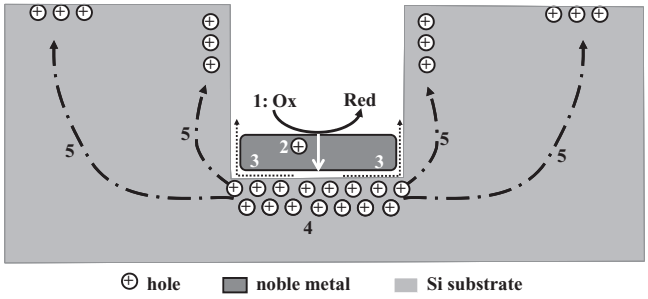

Figure 3. Scheme of processes involved in metal-assisted chemical etching. The numbers indicate the steps introduced in Section 2.5.

nanometers). As yet, there is no direct evidence in the literature proving unambiguously which of the two diffusion processes dominates during metal-assisted chemical etching.

2.5. The Overall Etching Process

Based on the published results, a picture describing the processes in metal-assisted chemical etching is tentatively suggested here (**Figure 3**): (1) The oxidant is preferentially reduced at the surface of the noble metal due to the catalytic activity of the noble metal on the reduction of the oxidant. (2) The holes generated due to the reduction of the oxidant diffuse through the noble metal and are injected into the Si that is in contact with the noble metal. (3) The Si is oxidized by the injected holes and dissolved at the Si/metal interface by HF. The reactant (HF) and the byproducts diffuse along the interface between the Si and the noble metal. (4) The concentration of holes has its maximum at the Si/metal interface. Therefore, the Si that is in contact with the metal is etched much faster by HF than a bare Si surface without metal coverage would be. (5) The holes diffuse from the Si under the noble metal to off-metal areas or to the wall of the pore if the rate of hole consumption at the Si/metal interface is smaller than the rate of hole injection. Accordingly, the off-metal areas or sidewalls of the pore may be etched and form microporous silicon, analogous to the case of electrochemical or stain etching.

3. Influence of Noble Metals on the Etching

3.1. Deposition Methods of the Noble Metal

In metal-assisted chemical etching, Ag, Au, Pt, and Pd are the most frequently used noble metals. They can be deposited on the Si substrate via various methods, which include thermal evaporation,[74–76] sputtering,[21,33,77] electron beam (e-beam) evaporation,[78] electroless deposition,[50,51] electrode deposition,[45] focused-ion-beam (FIB)-assisted deposition,[79] or spin-coating of particles via other methods.[44] To obtain patterned structures of Si by metal-assisted chemical etching, physical deposition in vacuum (e.g., thermal evaporation, sputtering, and e-beam evaporation) is favorable because the morphology of the resulting noble metal film can more easily be controlled in these methods. Details are described in Section 7. Electroless deposition is a simple method for the deposition of noble metals and is usually utilized to deposit noble metals if there is no strict demand on the morphology of the resulting etched structures. The metal deposited by FIB-assisted deposition is usually accompanied by contamination with gallium and amorphous carbon and the etching behavior is not predictable.[79]

Various plating solutions containing noble metal ions can be used to deposit noble metals electroless onto a Si substrate. The plating is a typical galvanic process, as reviewed by Ogata et al.[80] Briefly, the ions of the noble metal inject holes into the valence band of the Si substrate. In this process the metal ions are reduced and form nuclei on the surface of the Si. In parallel, holes injected into the Si substrate oxidize the Si to Si oxide.

The discussion here will be focused on plating solutions composed of HF and noble metal ions because the plating under such solutions is, simultaneously, a metal-assisted chemical etching process. Dendrite structures of the deposited metal formed when a Si substrate was immersed in a solution containing HF and M^{n+} (M = Ag or Au) for a relatively long time (e.g., longer than 30 min), in addition to the etching of the Si substrate (**Figure 4b**).[36] It was difficult to deduce the detailed formation mechanism of the metallic dendrites and the etching behavior that occurs in this system because of the thick layer of dendrite structure covering the etched Si structures. Because Si etched in $HF/AgNO_3$ solution[36] and in $HF/KAuCl_4$ solution[81] showed similar etched structures and a similar dendrite structure of the metal, only the experiments exploring the formation mechanism of dendrite structures in $HF/AgNO_3$ will be introduced here.

A galvanic cell was established by immersing a Si substrate into the $HF/AgNO_3$ solution because the electrochemical potential of Ag^+/Ag was more positive than the Fermi energy of the Si substrate (Figure 1c).[51] Holes were injected into the valence band of Si from Ag^+. The Ag^+ was reduced to elemental Ag forming nuclei (Figure 4a).[36,82,83] With increasing etching time the Ag nuclei grew into large particles. Simultaneously, the holes injected into the valence band of Si via Ag particles facilitated the local oxidation and dissolution of Si atoms underneath the Ag particles. With the dissolution of Si atoms underneath the Ag particles, the particles sank into the Si substrate. The charge transfer preferentially happened at the etching front, the interface between Si and the deposited Ag particle. Therefore, no new Ag nuclei emerged on the sidewall of etched pores and the Ag^+ was preferentially reduced forming Ag particles at the bottom of the etched pores. Accordingly, the Ag nuclei grew into dendrite structures (Figure 4b,c). By varying the concentration of $AgNO_3$ and HF, the diameter of the resulting Si nanowires (arising from overlapping pores) could be roughly tuned.[37]

The morphologies of Pt and Cu films electroless deposited from a HF-containing plating solution look different from those of Ag and Au. With increased etching time Pt and Cu tended to form a dense film on the surface of the Si substrate[84] rather than dendrite structures. The dense metal film further hindered the access of HF to the surface of the Si substrate and therefore blocked the further etching of the Si substrate.[51]

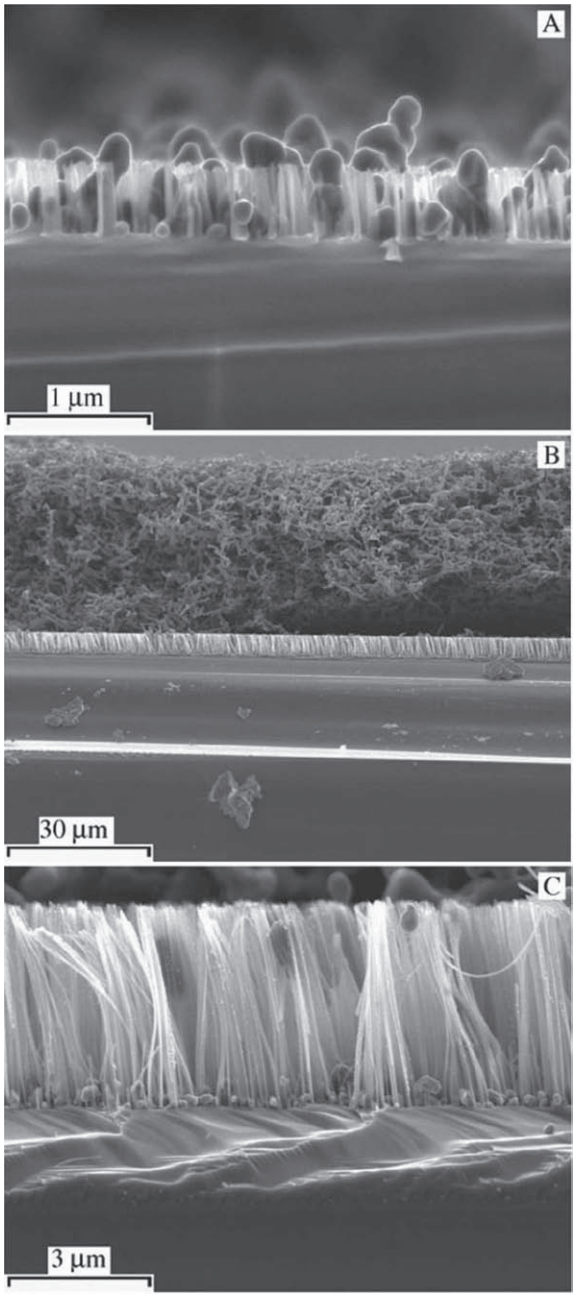

Figure 4. Cross-sectional scanning electron microscopy (SEM) images of p-type Si (111) substrates etched with $HF/AgNO_3$ for a) 5 min and b,c) 30 min. Adapted with permission.[36] Copyright 2006, Wiley-VCH.

Usually, plating solutions containing HF and ions of Pt or Cu can be used to deposit Pt or Cu particles but not to etch Si substrate into wires or pores.

3.2. Type of Metal

The morphologies of the etched structures vary with the type of noble metal if isolated particles are used for metal-assisted chemical etching. Usually, straight pores form if isolated Ag or Au particles are used to assist the etching of a Si substrate (**Figure 5a,b**).[38,48] The behavior of Pt particles is somewhat complex. Defined straight pores (Figure 5c) or helical pores induced by electroless deposited Pt particles were reported by Tsujino et al.[38,57] In contrast, it was demonstrated that Pt particles deposited by electroless plating[51] or sputtering[56] moved randomly during the etching, resulting in curvy pores without a uniform etching direction (Figure 5d).

The specific type of noble metal influences the etching rate. The rate of etching assisted by Pt was much faster than that assisted by Au.[33] Moreover, the pores in or wires on substrates etched in the presence of Pt were usually surrounded by a porous layer,[34,38] while no observable porous layer was found around the pores or wires etched from Au-coated[38] or Ag-coated[57] substrates under otherwise identical conditions. The difference in the etching rate and morphologies of the etched structures has not yet been well-explained in literature. The difference in the catalytic activity of the noble metal for the H_2O_2 reduction might be a possible reason, although there is no literature directly comparing the catalytic activities of Pt, Au, and Ag particles on Si substrates for the H_2O_2 reduction. As introduced in Section 2.3, hole injection is necessary for the etching of Si. When more holes are injected, the etching is faster. As is introduced in Section 4.2, when more holes are injected, the possibility that holes diffuse from the etching front to the sidewall of the etched structure (e.g., pores or wires) increases, favoring the formation of a microporous structure on the sidewalls of etched structures.

3.3. Shape of the Metal and Distance Between Metals

The morphologies of the resulting etched structures would usually be defined by the shape of the metal catalyst because the Si under metal catalyst is etched much faster than Si without metal coverage. In **Figure 6** some typical morphologies of noble metal catalyst and the morphologies of the resulting etched structures are sketched. Well-separated noble metal particles (Figure 6a) usually result in well-defined pores (Figure 6b), whereas the etched structures might evolve from pores into wall-like or wire-like structures (Figure 6d) when the distances between noble metal particles decreases (Figure 6c). Discontinuous patches (Figure 6e) cause wall-like or wire-like structures with a broad distribution of cross-sectional shapes and spacings (Figure 6f). Continuous films with a few holes (Figure 6g) lead to well-defined wires with more uniform cross-sectional shapes and spacings (Figure 6h). If the metal film contains orderly distributed pores with uniform diameters and cross-section shapes (Figure 6i), the Si substrate will be etched into an array of Si nanowires with identical cross-sectional shapes and spacings (Figure 6j).

In addition to the morphology, the distance between metal catalyst particles or patches strongly influences the morphology of the etched structures. It was shown that well-separated Ag particles from electroless plating catalyze the etching of isolated pores.[57] In contrast, if the Ag particle density is sufficiently high so that the Ag particles overlap (e.g., due to an increase in plating time), then isolated wire structures were obtained.[51] Even if the Ag particles do not overlap, but are sufficiently close

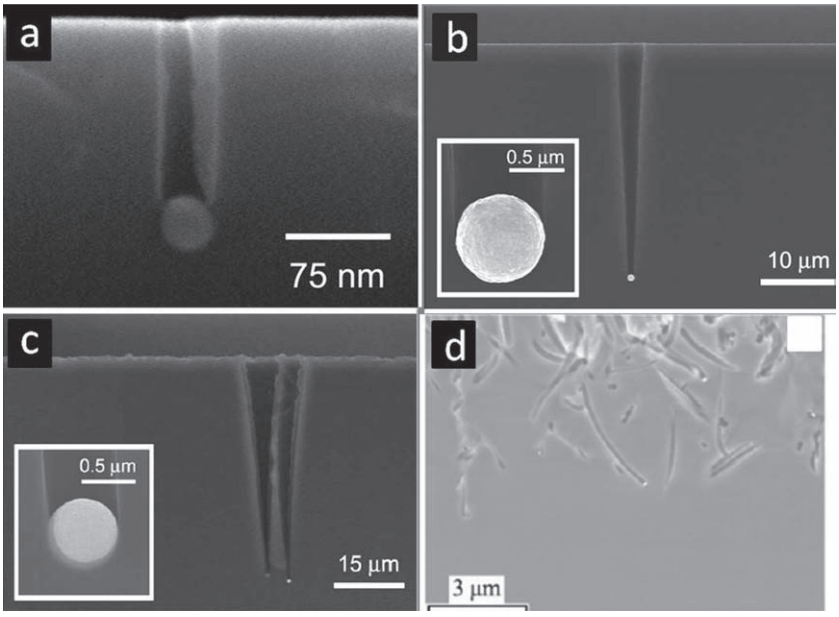

Figure 5. Typical morphologies of etched structures with: a) Ag particle. Adapted with permission.[48] Copyright 2007, Elsevier. b) Au particle. Adapted with permission.[38] Copyright 2008, RSC. c,d) Pt particle. c) Adapted with permission.[38] Copyright 2008, RSC. d) Adapted with permission.[51] Copyright 2006, Wiely-VCH.

to each other, Si nanowires might also be formed. A single Au or Ag particle sinks straight into the Si substrate and etches the Si substrate, forming a pore. The pore might be widened because of the following reasons. First, the Si without metal is etched as well due to the diffusion of injected holes from the etching front to the side wall of the pore,[34,39] as will be introduced in Section 4.2, although the etching rate is much smaller than for Si with metal coverage. Second, the dissolution and redeposition of Ag on the sidewall of the etched pores also contributes to the thinning of the pore wall.[21,41,77] Third, the Si without noble metal coverage is etched slowly in the etchant.[62] Accordingly, the etched pore usually exhibits a cone shape, with the diameter of aperture on the surface of the substrate larger than the initial diameter of the noble metal particle.[38] If the distances between the noble metal particles are sufficiently small, the cone-shape pores overlap, forming Si nanowires or nanobelts.[36,51,85]

The nominal thickness of metal films deposited by physical methods in vacuum influences the morphologies of the etched structures. Fine pore structures formed in the etching using a 3-nm-thick Au film as a catalyst, while a 7-nm-thick Au film led to a columnar structure.[56] A layer of Ag film with a nominal thickness of 5 nm led to porous pore structures (**Figure 7a1–3**), while a Ag film with a nominal thickness of 20 nm (Figure 7b1–3) or 50 nm (Figure 7c1–3) led to Si nanowires.[74] The morphology of the Ag or Au film deposited by thermal evaporation or sputtering depends on its nominal thickness. It varies with an increase in nominal thickness from isolated particles or patches, via partially interconnected patches, to a continuous film with pores and finally to a continuous film without pores.[21,74] Therefore, the different morphologies of structures from the etching with metal sof different thicknesses can be attributed to the different shapes of distances between, and packing manners of the metal particles, which are determined by the thickness of metal.

3.4. Shape Evolution and Movement of Metal Particles During Etching

Although it is termed a catalyst in literature, the noble metal is possibly oxidized and dissolved into the solution, depending on the relative relationship between the electrochemical potential of the oxidant and the noble metal. Pt and Au particles were stable in the etchant even for concentrations of H_2O_2 as high as 8.1 M and they maintained their initial shapes during the etching.[34] Meanwhile, it was proposed that different facets on the surface of Pt particles[34] or irregularly shaped Au[38] or Ag[48] particles exhibited different catalytic activities for the etching of the Si substrate. Whether this facet-dependent catalytic activity is at least partly responsible for unexpected etching structures, such as helical pores from Pt particles[34] and spiral pores from Au particles[38] remains unclear at present.

In contrast, it has been demonstrated that a dissolution and/or re-deposition process occurred for Ag particles, due to the relatively low electrochemical potential of Ag. Ag particles with irregular shapes transferred into spherically shaped ones after a 30 min etching.[57] Correspondingly, the characteristics of the etched morphology varied with time. At the initial stage of the etching, the irregularly shaped Ag particles randomly moved in various directions, possibly due to different catalytic activities on different facets, resulting in a porous structure. With increasing etching time, the Ag particles became spherical and started catalyzed etching along the vertical [100] directions, leaving behind straight cylinder pores.[57] In solution with 0.18 M H_2O_2, the dissolution of Ag particles was apparent.[38] Ag particles experienced a drastic size reduction, accompanied by the formation of many small-diameter Ag particles. Accordingly, the etched structures appeared as large cone-shaped pores, induced by the original Ag particles, surrounded by many small-diameter pores, which resulted from the catalytic etching of re-deposited small-diameter particles.[38]

Because of its relatively low electrochemical potential, Cu is easily oxidized even in an etchant containing a mild oxidant such as Fe^{3+}.[51] Therefore, Cu particles loaded on the Si substrate vanished in a typical etchant in a couple minutes, leaving the open question of whether Cu can catalyze the etching of Si, although it has been recently reported that Cu can catalytically reduce H_2O_2.[86]

Due to their stability in the etchant solution, Au meshes allow the fabrication of Si nanowires with ultralarge aspect-ratios (e.g., larger than 200).[78] When fabricating Si nanowire arrays with a Ag mesh, which can slowly be dissolved by the etchant, new pores may form in the mesh leading to unintended Si nanowires at the location of these pores.

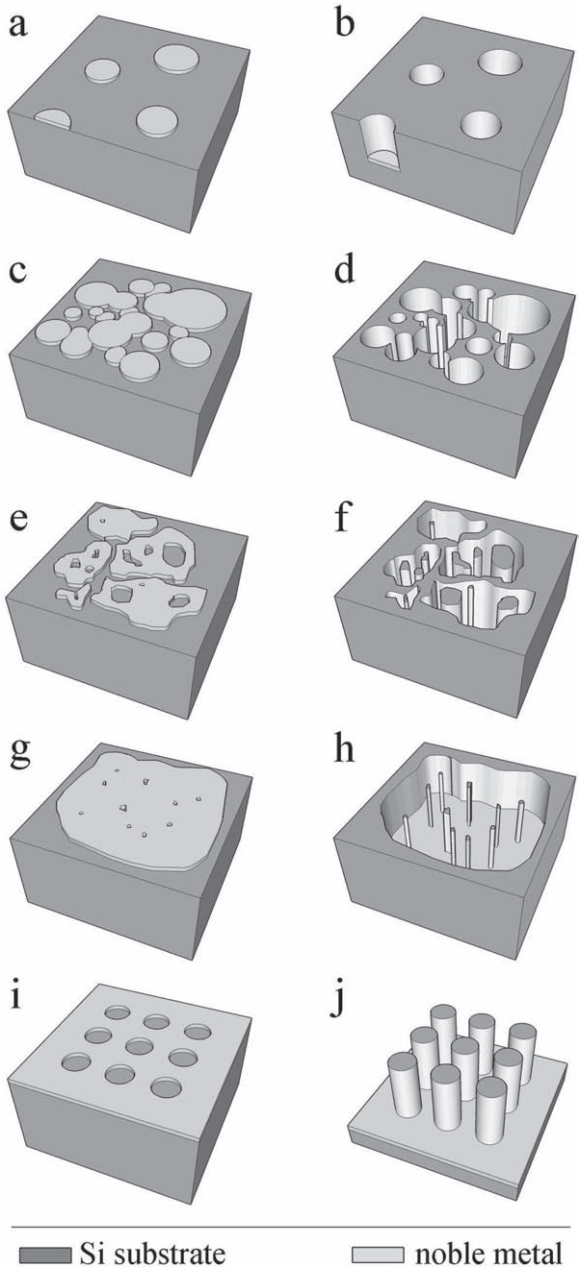

Figure 6. Scheme of typical morphologies of etched structures (right column) induced by metal catalysts with differently shaped noble metals (left column).

3.5. Interaction Between Noble Metal Particles

Isolated Ag particles or Ag patches tended to move along the same direction in metal-assisted chemical etching of a (110) substrate[21] on which the etching was intrinsically anisotropic. At the initial stage of etching, each patch moved along an allowed <100> direction (i.e., $[\bar{1}00]$ or $[0\bar{1}0]$) at random (**Figure 8a**). With increased etching time, some particles switched their initial directions and moved in the same direction as their neighbors. Hereby the substrate developed into domain structures, within which the etching occurred in the same direction. Moreover, the Ag particles near the domain boundary switched their directions in sequence (Figure 8b), resulting in the coalescence of domains and the enlargement of the size of domains. This phenomenon implies that there is a distance-dependent interaction between the silver particles that makes the silver particles cooperatively move in the same direction. The details of this interaction are not yet understood and are tentatively attributed to the image forces between the silver particles[87] and/or the influence of band bending at the Ag/Si interface from neighboring silver particles and, thus, the influence of carrier transfer through the silver/Si interface.[88] As a result of such interactions, the size of domains can be larger than 100 μm in samples etched for 10 min.[21]

It was speculated that the etching direction depends not only on the crystallographic orientation of the Si substrate, but also on the morphology of the noble metal particles used to catalyze the etching.[34,38,48] This assumption is reasonable because copious amounts of literature have revealed that the catalytic activity of a noble metal is determined by the facets it exposes. This assumption has been tentatively used to explain the origin of non-straight pores. Pore etching induced by an aggregation consisting of two Au particles with different diameters deviated from the vertical direction, suggesting different etching rates at particles of different diameters. If the number of Au particles in the aggregation was sufficiently large (e.g., larger than 10) the pore induced by this aggregation proceeded along the crystallographically preferred direction, probably due to the cancellation of different lateral components.[38]

4. Influence of the Etchant on the Etching

4.1. Type of Oxidant

Various oxidative agents have been mixed with HF to etch noble-metal-loaded Si substrates, including $AgNO_3$,[36,89,90] $KAuCl_4$ or $HAuCl_4$,[81] K_2PtCl_6 or H_2PtCl_6,[84] $Fe(NO_3)_3$, $Ni(NO_3)_2$,[51,75] $Mg(NO_3)_2$,[51] H_2O_2,[21,33,76,77,84] $Na_2S_2O_8$,[47] $KMnO_4$,[47] $K_2Cr_2O_7$,[47] O_2 bubble, or O_2 dissolved in H_2O.

When $AgNO_3$, $KAuCl_4$/$HAuCl_4$, or K_2PtCl_6/H_2PtCl_6 is used, the metal ions are reduced to particles, dendrite structures, or a film depending on the etching time, parallel to the oxidation and dissolution of the Si substrate. The processes involved in the etching of Si with HF and this type of metal were already introduced in Section 3.1.

The dissolution of Si in HF solution generates SiF_6^{2-}, with maximum concentration at the etching front. Fluorosilicate precipitates will form at the etching front in the etchant if the ionic product exceeds the solubility product. For example, in an etchant containing $KMnO_4$ or $K_2Cr_2O_7$, with concentration higher than 0.1 M, spherical white particles formed on the surface of Si. These particles were K_2SiF_6 precipitates, as confirmed by X-ray diffraction. Similarly, precipitates of K_2SiF_6 were found during stain etching of Si in HF solution containing a high concentration of K^+[60,61] and during laser-assisted formation of porous Si in a HF solution containing a high concentration of K^+.[91] No precipitation formed on the surface of Si etched in HF/$Na_2S_2O_8$ solution, even if the concentration of $Na_2S_2O_8$ was

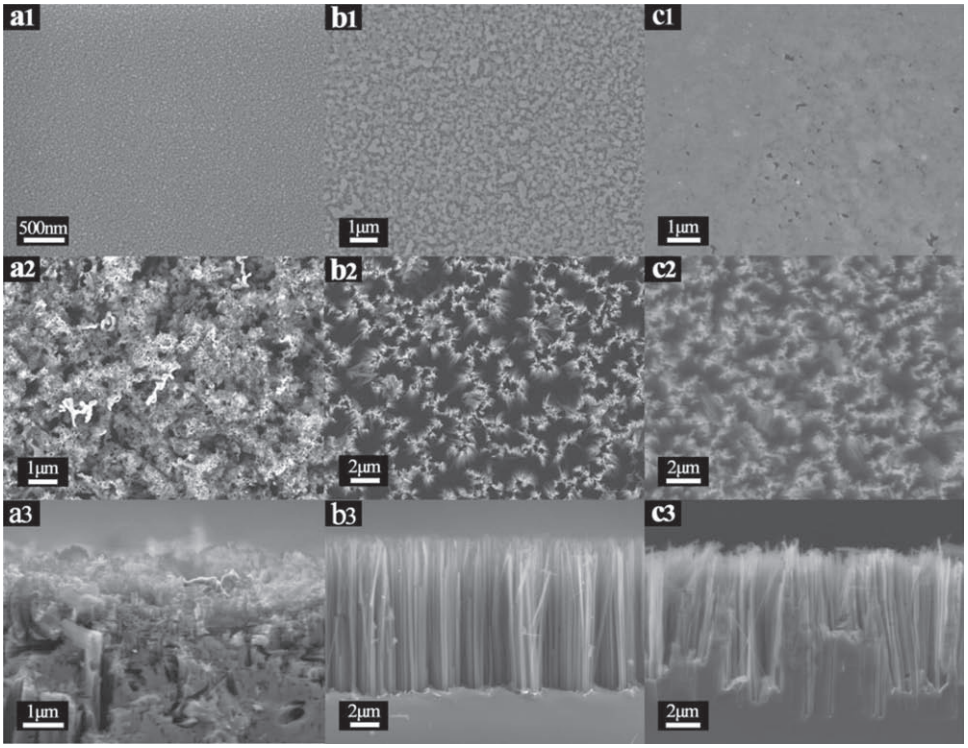

Figure 7. Plan-view SEM images of a1) 5-nm-thick, b1) 20-nm-thick, and c1) 50-nm-thick Ag film on a Si substrate. Plan-view SEM images of structures etched from a substrate loaded with a2) 5-nm-thick Ag, b2) 20-nm-thick Ag, and c2) 50-nm-thick Ag. Cross-sectional SEM images of structures etched from a substrate loaded with a3) 5-nm-thick Ag, b3) 20-nm-thick Ag, and c3) 50-nm-thick Ag. Adapted with permission.[74] Copyright 2006, AIP.

higher than 0.3 M[47] because the solubility of Na_2SiF_6 is approximately 1 to 2 times higher than that of K_2SiF_6.[92] Precipitates of $MSiF_6$ (M = Fe, Ni, Mg) have not been reported because of the very high solubility of the fluorosilicate in the solution.

It should be mentioned specifically that $Fe(NO_3)_3$,[58,59] $KMnO_4$,[60] $KBrO_3$,[60,61] and $K_2Cr_2O_7$[60] were also used as oxidants in stain etching of Si, suggesting that for the metal-assisted chemical etching of Si in HF/oxidant (oxidant = $Fe(NO_3)_3$, $KMnO_4$, $KBrO_3$, or $K_2Cr_2O_7$) solution the etching occurs not only at the Si/metal interface but also at the surface of the Si without metal coverage. The Si substrate loaded with isolated particles and polystyrene (PS) sphere mask was etched into small pillars or disks in HF/$Fe(NO_3)_3$ solution.[75] It is apparent that in HF/$Fe(NO_3)_3$ solution the Si without PS protection was etched, independent of the position of the Ag particles. In contrast, the Si substrate loaded with isolated noble metal particles was etched into deep pores in HF/H_2O_2 solution (Figure 5).[38,48] It was shown that etching of a Si substrate loaded with Ag particles in $Na_2S_2O_4$ resulted in a very rough porous structure, which clearly looked different from that etched in an etchant composed of HF and H_2O_2.[47]

4.2. Concentration of Etchant

The concentrations of H_2O_2 and HF affect not only the etching rate, but also the morphologies of the etched structures. A straight pore induced by a Pt particle in an etchant with low HF concentration (HF(50%):H_2O_2(30%):H_2O = 2:1:8; v:v:v) was surrounded by a cone-shaped porous structure. The porous region on the surface of the Si substrate extended over a region with a diameter larger than 1 μm, while the diameter of the central straight cylinder pore was less than 50 nm. A fourfold increase in HF concentration (HF(50%):H_2O_2 = 10:1; v:v) dramatically reduced the size of the surrounding porous structure to less than 100 nm.[34] In a solution with 0.15 M $Na_2S_2O_8$, Ag plated Si was etched into a porous structure with a rough surface and a wide distribution of the pore diameters, whereas a 0.3 M $Na_2S_2O_8$ etchant (with the other etching conditions kept constant) led to a much smoother etched surface.[47] The author attributed the smoother surface etched from a solution with higher $Na_2S_2O_8$ concentration to a higher hole injection rate and subsequently more uniformly distributed holes compared to the case with a lower $Na_2S_2O_8$ concentration.

Chartier et al. systematically studied the influence of the HF/H_2O_2 ratio on the etching rate and on the etched morphologies of Si substrates (p-(100), 1–2 Ω cm) on which isolated Ag particles were deposited by electroless plating.[39] The morphologies of the etched structures were determined by the parameter ρ, defined as [HF]/([HF]+[H_2O_2]) (**Figure 9**). With 100% > ρ > 70%, Ag particles induced straight cylinder pores, the diameters of which match well those of the Ag particles at the bottom. With 70% > ρ > 20%, cone-shaped pores formed. The diameter of the pore tip was the same as the diameter of the Ag particle located there, while the opening of the pore at the surface of the Si substrate had a diameter larger than that of the Ag particle. For

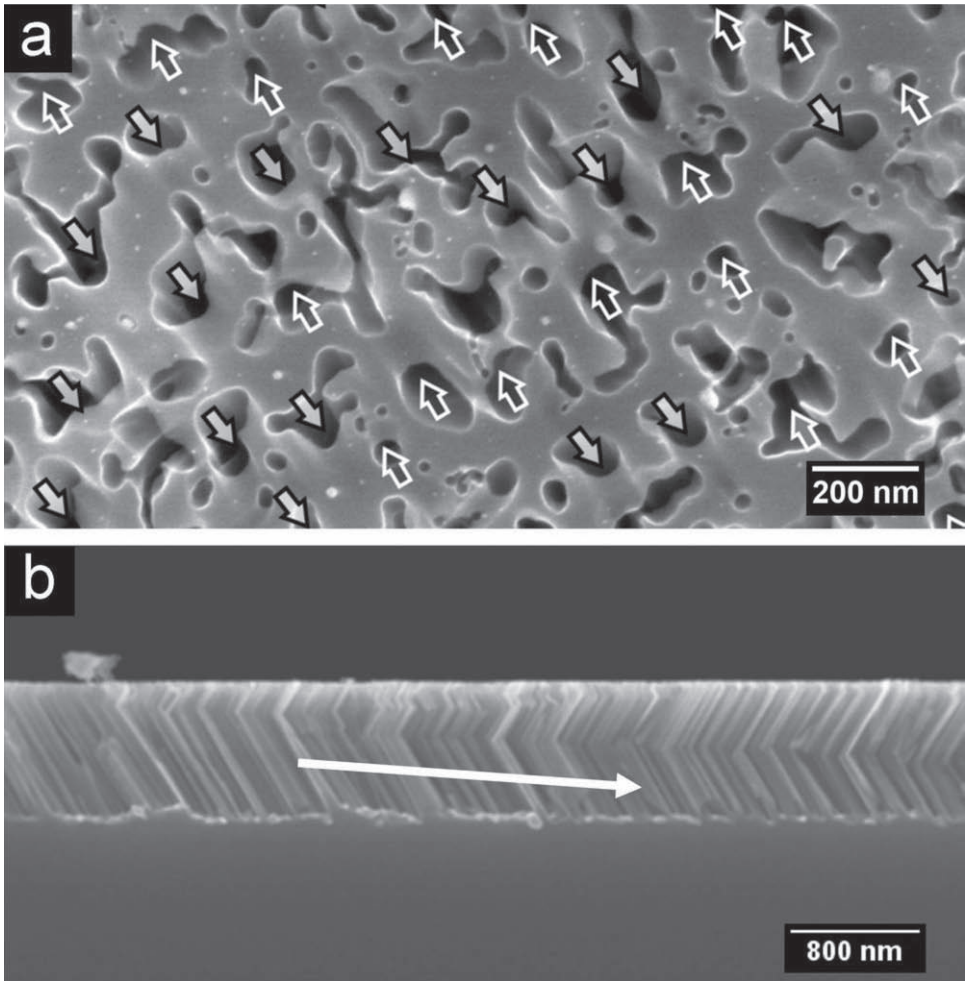

Figure 8. a) Plan-view SEM image showing the morphology of a (110) Si substrate etched with Ag particles with large separation distance. The open and solid arrows indicate different etching directions. b) Cross-sectional SEM image showing that the Ag particles switch their movement direction from left to right in sequence during the etching. The arrow shows the propagation direction. Adapted with permission.[21] Copyright 2009, ACS.

ρ below 30%, the cone-shaped pores were surrounded by microporous Si, which looked similar to the structure etched with Pt particles in low HF concentration.[38] With 20% > ρ > 9%, Si evolved into crater structures with opening diameters of several micrometers. With 9% > ρ > 0%, neither porous nor crater structures formed and a macroscopically smooth but nanoscopically pitted surface developed.

The relationship between etching morphologies and ρ was explained as follows:[39] For 100% > ρ > 70% (i.e., a high percentage of HF), the etching rate was almost completely determined by the concentration of H_2O_2 and nearly all holes generated at the Ag/Si interface at the pore tip were locally consumed because there was sufficient HF available to dissolve Si (or SiO_x, if this occurs as an intermediate reaction product). When ρ was less than 70%, the etching rate was determined by the concentration of HF. In this case, the consumption rate of the holes at the pore tip was smaller than the generation rate. Accordingly, unconsumed excess holes could diffuse away from the tip to the side wall of the pore. Hence, microporous Si formed on the side wall of the pore. With very small ρ, or very high H_2O_2 concentration, holes diffusion was pronounced and the diffused holes came to every exposed surface of Si substrate. Consequently, oxidation and dissolution of Si occurred everywhere and the etching was isotropic and independent on the location of Ag particles, resulting in a polished surface.

For 70% > ρ > 20%, the model by Chartier et al. did not explain why the diffused holes were likely to oxidize Si on the side wall and why the cone-shaped microporous region formed.[39] Sullivan et al. simulated the potential distribution in a Si substrate around a pore with a metal at the bottom and depicted an inhomogeneous distribution of the potential around the side wall of the pore.[88] This result might help to explain the origin of the cone-shaped microporous region surrounding the etched pore.

In metal-assisted chemical etching of non-(100) substrates, the concentration of oxidant (e.g., H_2O_2, $Fe(NO_3)_3$) affects the etching direction, resulting in vertical etching or crystallographically preferred <100> etching. These phenomena will be introduced in detail in Section 6.1. Another influence of the oxidant concentration on the etching is the dissolution of the metal during the etching, which is discussed in detail in Section 3.4.

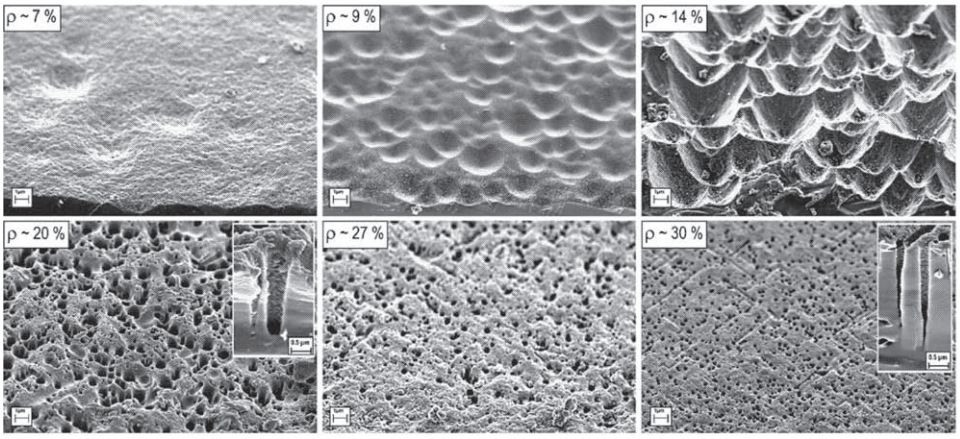

Figure 9. SEM images of *p*-Si (100) substrates etched in solutions of different ρ values. Adapted with permission.[39] Copyright 2008, Elsevier.

4.3. Diffusion of Etchant

The effective etching rate is not only directly affected by temperature but also by factors that influence the diffusion of agent and byproduct into or out of the etched pores. Lee et al. observed that the etching rate of pores induced by an aggregation composed of a large number of Au particles was apparently larger than that induced by a single Au particle or an aggregation composed of two Au particles. The faster etching rate was attributed to the larger cross-section of the pores, which enabled the efficient diffusion of HF, H_2O_2, and SiF_6^{2-} into or out of the etching front.[38] An efficient diffusion of agent and byproduct can also be achieved by stirring the etching solution.

5. Influence of Temperature and Illumination on the Etching

It has been reported that the length of Si nanowires fabricated by metal-assisted chemical etching in HF/$AgNO_3$ solution or HF/H_2O_2 solution increased approximately linearly with the etching time. Cheng et al. systematically studied the relationship between the etching time and the lengths of Si nanowires etched at different temperatures. With a temperature in the range of 0 °C to 50 °C, a linear relationship between length of nanowire and etching time at all temperatures was confirmed (**Figure 10a**). The observed etching rate increased with increasing etching temperature. From the etching rates at different temperatures, Cheng et al. obtained an apparent activation energy of 0.36 eV for the formation of Si nanowires on a (100) Si substrate via the corresponding Arrhenius plot (Figure 10b).[93]

Metal-assisted chemical etching of p-(100) and n-(100) type Si substrates with the same resistivity (1–10 Ω cm) has been conducted in the dark, with room light illumination, and with illumination from a 20 W bulb. Etching of p- and n-type substrates occurred successfully both in the dark and with illumination. For the same etching times, the difference between etching depths in the dark and with room light illumination was less than 5% for both p- and n-type substrates, while the etching depth during illumination with a 20 W bulb was about 1.5 times the etching depth in the dark or with room light illumination, clearly demonstrating the influence of illumination on the etching rate.

The electrochemical potential of the oxidant (H_2O_2) is much more positive than the valence band of Si (Figure 1b).[35] Therefore, holes can be injected into the valence band of Si, independent of the doping type of the substrate.[35] Consequently, illumination is not required for metal-assisted chemical etching of an n-type Si substrate. Due to the catalytic activity of the noble metal, reduction of H_2O_2 is fast and copious numbers of holes are injected into Si. If the intensity of illumination is low (e.g., room light illumination), the number of photoexcited holes is much smaller than the number of holes injected from the reduction of H_2O_2 and no obvious difference in etching rate is observed. If the intensity of illumination is sufficiently high so that the concentration of photoexcited holes is comparable

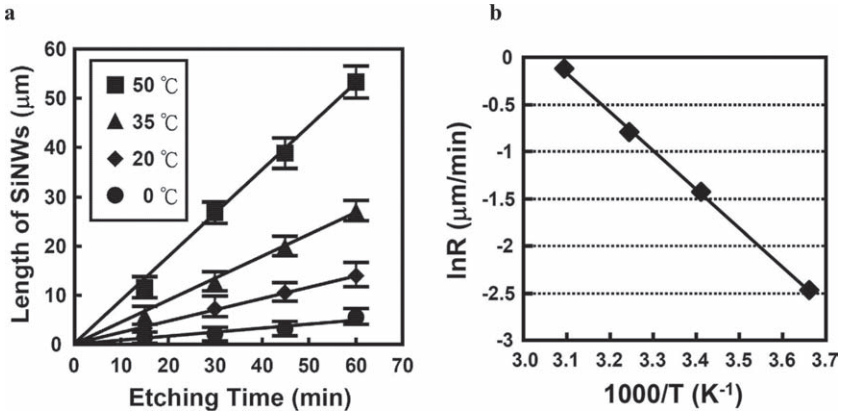

Figure 10. a) Relationship of length of Si nanowires and the etching time at different temperatures and b) Arrhenius plot of the formation rate versus reciprocal absolute temperature. Adapted with permission.[93] Copyright 2008, ECS.

with or higher than the concentration of holes injected from H_2O_2, faster etching occurs.

6. Influence of Intrinsic Properties of the Si Substrate on the Etching

6.1. Orientation

It has been speculated that the metal-assisted etching is isotropic and the noble metal always catalyzes the etching along the vertical direction relative to the substrate surface. The experiments in early years showed that, indeed, in (100) and (111) substrates the etching proceeded along the vertical direction.[36,50] However, it was later revealed that non-vertical etching occurred in (111) and (110) substrates, resulting in slanting, aligned Si nanostructures.[5,37,38,40,94,95] Confusingly, the etching of non-(100) substrates exhibited different and partly contradictory results, showing an etching direction in vertical direction, non-[100] directions[5,36,37,40,50,94] or a switch of etching direction from the vertical direction to one of the <100> directions.[37,40]

The non-vertical metal-assisted chemical etching (i.e., the anisotropic etching in certain preferred crystallographic directions) was ascribed to the back-bond breaking theory,[40,96] which had already been used to explain the anisotropy in the anodic HF etching of Si[97] and the etching of Si in alkaline solution.[24] For the oxidation or dissolution of a Si atom on the surface of a substrate, it is necessary to break the back-bonds of the surface atom that connects to the underneath atoms. The stronger the back-bond strength, the more difficult to remove the surface atom. The number of back-bonds of a Si atom on the surface is determined by the crystallographic orientation of the substrate. Each atom on the surface of a (100) substrate has two back-bonds, while an atom on the (110) or (111) surface has three back-bonds.[98] Due to the different back-bond strength, the Si atom on the (100) surface plane is the most easily removed, and the etching occurs preferentially along the <100> directions.

However, the influence of the etching anisotropy on the etching rate of a Si substrate (measured as the change in the etching depth vertically to the surface) remains puzzling. Huang et al. found that in the same etchant and for the same etching time, the etching depth of a (110) substrate etched along the <100> directions was almost the same as the etching depth of the same substrate etched along the [110] direction.[21] Zhang et al. found similar phenomena in the etching of (111) and (100) substrates with a different doping type but the same doping level, despite the different etching direction (**Table 1**).[41]

The anisotropy could be reduced or eliminated by varying the concentration of oxidant in the etchant,[20] although the metal-assisted chemical etching of Si is intrinsically anisotropic along the crystallographically preferred <100> directions. The back-bond strength theory implies that the anisotropy might be reduced or eliminated if the back-bond strength is weakened. In the etching of Si in alkaline solution, it has been revealed that the addition of oxidant into the alkaline etchant could reduce the anisotropy.[99] Hillock structures, which are a characteristic of (100) Si substrates etched in alkaline solution, almost vanished and the etched substrate showed a relatively smooth surface. It was speculated that the dangling bonds of the surface Si atoms varied from –H in alkaline solution to –OH with the addition of oxidant, and the –OH surface bond effectively reduced the strength of the back-bond, accordingly reduced the anisotropy, enabling a reduction of the hillock structures.[99] These results suggest an approach to reduce the strength of the back-bonds by addition of an oxidant.

This approach was applied to the metal-assisted chemical etching of non-(100) Si.[20] Specifically, a (111) substrate loaded with isolated Ag particles (**Figure 11a**) was etched in solutions consisting of HF and H_2O_2 with different concentrations. In the solution with low oxidation concentration ($[H_2O_2]$ = 2 mM), the etching proceeded along crystallographically preferred <100> directions (Figure 11b). With the concentration of H_2O_2 increased to 20 mM, the etching direction changed into an inclined direction between the vertical [111] direction and crystallographically preferred <100> directions (Figure 11c). The etching direction completely changed to the vertical [111] direction if the concentration of H_2O_2 exceeded 100 mM (Figure 11d).[20] The etching direction on the (111) substrate loaded with isolated Ag particles in an etchant containing HF and $Fe(NO_3)_3$ also depended upon the concentration of $Fe(NO_3)_3$. It occurred along <100> directions in a solution with low $Fe(NO_3)_3$ concentration (13.5 mM) and along the vertical [111] direction in solution with high $Fe(NO_3)_3$ concentration (135 mM).[20] An oxidant-concentration-dependent etching direction occurred also in the etching of a (110) substrate (1–10 Ω cm) with an etchant containing HF and H_2O_2. In an etchant with $[H_2O_2]$ = 400 mM, etching occurred along inclined <100> directions, while etching proceeded in the vertical [110] direction in an etchant with $[H_2O_2]$ = 1 M.[20] These results imply that the effect of an oxidant-concentration-dependent etching direction is a general feature occurring in non-(100) Si substrates. By this approach, orientation-modulated pores or nanowires can be fabricated by etching a Ag-particle-loaded non-(100) Si substrate periodically in solutions with high and low oxidant concentration.[20]

The observed switch of the etching direction from the [111] direction to <100> directions in literature[5,36–38,40,50,94,95] can be

Table 1. Etching depth and etching direction of p- and n-type Si substrates with different doping type and resistivity in different etchants. Etchant I is composed of 4.8 M HF and 0.4 M H_2O_2; Etchant II is composed of 4.8 M HF and 0.15 M H_2O_2. Adapted with permission.[41] Copyright 2008, ACS.

Substrate	p (100)	p (111)	n (100)	n (111)	p (100)	p (111)
Resistivity [Ω cm]	7–13	8–13	7–13	4–8	0.003–0.005	0.004–0.008
Etching Depth [μm]	30	30	45	50	20	20
Etching Direction	[100]	[100]	[100]	[111]	[100]	[100]
Etchant	I	I	I	I	II	II

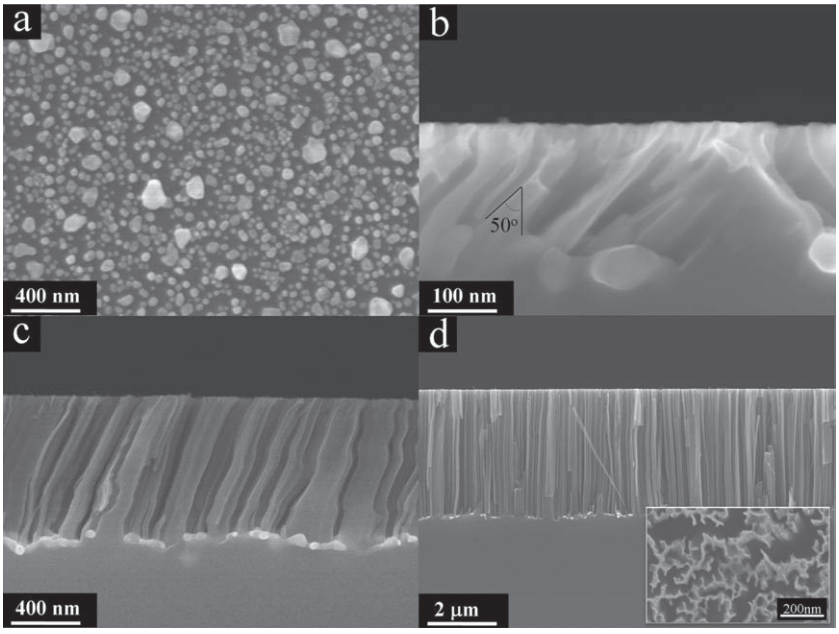

Figure 11. a) Plan-view SEM image of a (111) Si substrate loaded with isolated particles via electroless plating. Cross-sectional SEM images of Ag-loaded (111) Si substrate etched in an etchant composed of HF (5.6 M) and b) H_2O_2 (2 mM), c) (20 mM), and d) (100 mM). Inset in (d) shows a plan-view SEM image of the sample shown in (d). Adapted with permission.[20] Copyright 2010, ACS.

explained by a decrease in oxidant concentration during the etching.[20] In metal-assisted chemical etching of Si, the concentration of oxidant near the etching front is smaller than that in the bulk solution because of the consumption of oxidant. With increasing etching time, the etching front proceeds deep into the Si substrate and the oxidant near the etching front has to be supplied by oxidant diffusion from the bulk solution into the deep pores. If the rate of oxidant consumption is higher than the rate of oxidant supply, the concentration of oxidant at the etching front decreases with etching time. With decreasing concentration of oxidant, the anisotropy is increased and the etching direction changes from the initial vertical [111] direction (in a solution with initially high oxidant concentration) to inclined directions, and finally to the crystallographically preferred [100] directions.

In addition to the approach based on the oxidant concentration in the etchant, Huang et al. developed another approach to suppress anisotropy in metal-assisted chemical etching via control of the lateral size of the catalyst metal mesh.[21] For a (110) Si substrate (1–10 Ω cm) etched with isolated Ag particles (**Figure 12a**) in a solution with low oxidant concentration ($[H_2O_2]$ = 0.1 M), the etching of Si and the movement of Ag particles proceeded along inclined <100> directions (Figure 12b). The inclined <100> etching can formally be regarded as a vectorial addition of lateral (i.e., $[1\bar{1}0]$ or $[\bar{1}10]$) and vertical (i.e., $[\bar{1}\bar{1}0]$) etching, implying that the etching will occur along the vertical direction if the lateral etching of Si or the lateral movement of the Ag catalyst is restricted. The isolated noble metal particles could move freely during the etching, allowing the etching to proceed along the crystallographically preferred <100> directions. In contrast, if the noble metal particles are interconnected into a continuous film with pores (in other words, a noble metal mesh, Figure 12c), different parts of the mesh tend to move along the $[\bar{1}00]$ or $[0\bar{1}0]$ directions at random, possibly depending on defect sites on the surface of the substrate,[98] the shape or profile at the edge of the silver pores or the silver,[34,38,48] and the interaction between the substrate and the silver particles.[40] At the same time, there is a distance-dependent interaction between silver particles that makes the silver particles tend to move in the same direction. If this interaction extends over the entire mesh, the entire mesh does move in the same inclined direction during the etching, provided that the lateral size of the interconnected mesh is small. In contrast, if the lateral size of the mesh is sufficiently large (e.g., larger than tens of micrometers) so that the interaction cannot extend over the whole mesh, the different parts of the mesh maintain the tendencies to move

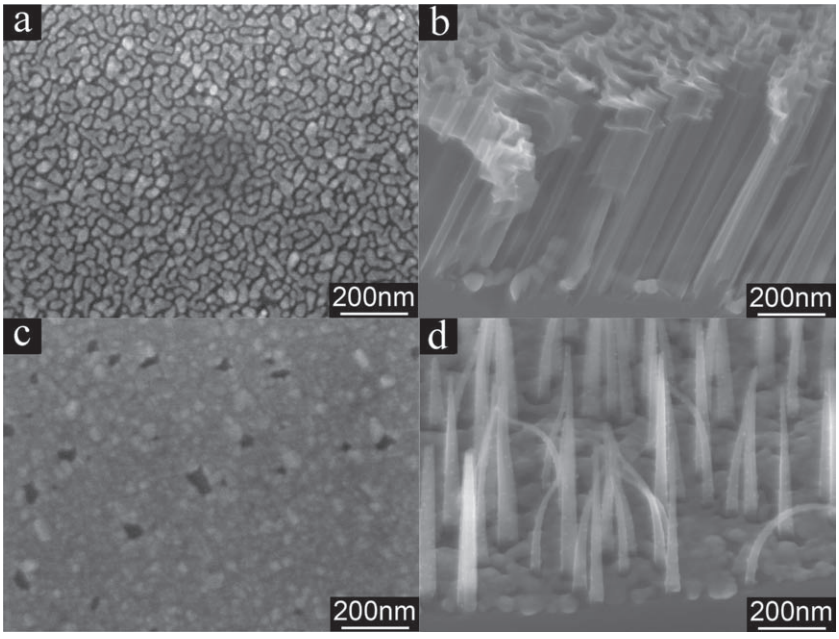

Figure 12. Plan-view SEM images of a (110) substrate loaded with a) isolated Ag patches and c) Ag film with pores. Bird's-eye-view SEM images showing the morphologies of etched structures from a substrate loaded with b) isolated Ag patches and d) Ag film with pores. Adapted with permission.[21] Copyright 2009, ACS.

along the allowable etching directions at random. However, the silver particles in the mesh are interconnected so that they cannot move freely as isolated particles. As a compromise among conflicting lateral etching directions ([$1\bar{1}0$] and [$\bar{1}10$]), the lateral movement of the large-area silver mesh is eliminated and the large-area silver mesh can only move in a common vertical direction ([$\bar{1}\bar{1}0$]), leading to vertically aligned[110] SiNWs (Figure 12d). The mechanism for the vertical etching was confirmed by the fact that the vertical etching could be converted to inclined etching due to a splitting of a large-area silver film into many smaller pieces induced by the dissolution of the silver during the etching.

6.2. Doping Type and Doping Level

Different conclusions concerning the relationship between etching rate and doping type or doping level of the Si substrate have been reported. Li et al. found that under identical conditions Au-covered regions on a p^+ (0.01–0.03 Ω cm) Si substrate and Au-covered regions on a p^- (1–10 Ω cm) substrate showed only small variations in pore size and etching depth,[33] while Cruz et al. reported that the etching depth in Au-covered regions of a p^- (10 Ω cm) Si substrate was 1.5 times larger than that of a p^+ (0.01 Ω cm) Si substrate, under identical conditions.[56] The reason for different etching rates for substrates with different doping levels remains unclear so far.

Concerning the doping type, Zhang et al. found that a p-type (7–13 Ω cm) substrate was etched more slowly than an n-ype (7–13 Ω cm) substrate. This relationship was valid for both (100) and (111) substrates. The etching depths of various substrates in the experiment of Zhang et al. are listed in Table 1.[41]

Besides influencing the etching rate, the doping level of the Si substrate also influences the morphology of the etched structures. With increasing doping level, Si nanowires resulting from metal-assisted chemical etching become rougher[26,41] and finally evolve into nanowires containing micro- or mesopores. Schade et al. found that Ag-assisted chemical etching of a highly doped n-type (0.001–0.006 Ω cm) Si substrate in aqueous solution of HF(4.6 M)/H_2O_2(0.22 M) resulted in a single-crystalline porous structure composed of crystalline Si, amorphous Si, and SiO_x with $x \leq 2$.[100] Hochbaum et al. found that etching of highly doped p-type Si substrates ($\rho < 0.005$ Ω cm) in aqueous solution of HF(5 M)/$AgNO_3$(0.01–0.04 M) led to single crystalline mesoporous Si nanowires (**Figure 13**). Interestingly, highly doped n-type Si substrates etched in the same solution produced only rough but solid nanowires, regardless of the dopant concentration.[101] In contrast, Zhang et al. did not get porous Si nanowires when they etched highly doped p-type Si (100) substrates (0.003–0.005 Ω cm) and highly doped p-type Si (111) substrates (0.004–0.008 Ω cm) in aqueous solution of HF(4.8 M)/H_2O_2(0.15 M) with Ag particles.[41] The dopant element of the substrate used by Zhang et al.[41] was not mentioned, so it is hard to deduce why a porous structure did not form in their experiment.

The etching behavior of the highly doped p-type Si substrate in the experiments of Hochbaum et al. is analogous to the etching phenomena reported by Li and Bohn et al.[33] In the experiments of Li and Bohn et al. the Au-coated area on a highly doped p-type Si substrate (0.01–0.03 Ω cm) was etched into a 350-nm-long columnar structure (Si nanowires) in HF/H_2O_2 solution and the off-metal area was etched into a mesoporous structure (≈3 nm) with an etching depth of 250 nm, while the etching depth in the off-metal area on a lightly doped Si substrate (1–10 Ω cm) was only ≈10 nm. Both p-type and n-type substrates exhibited similar etching behavior.[33]

Analogous to the porous structure on the sidewall of pores in lightly doped Si substrates,[39] it is suggested that the porous structure in highly doped Si substrates might originate from the diffusion of holes from the etching front at the Si/noble metal interface to the substrate without a noble metal during exposure to the etchant. This assumption is consistent with the result reported by Cruz et al.[56] Hochbaum et al.[101] proposed that the hole injection was favored in highly doped Si substrates

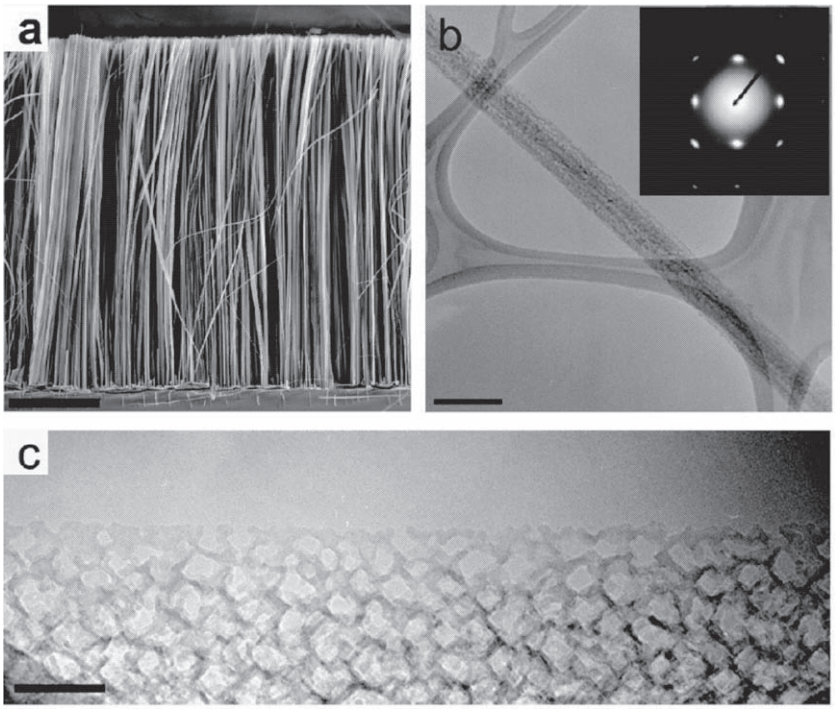

Figure 13. Structural characterization of porous silicon nanowires fabricated by metal-assisted chemical etching of highly doped p-type Si substrate. a) A cross-sectional SEM of the porous nanowire array. The nanowires are vertically oriented and part of a monolithic silicon crystal including the remaining wafer from which they were etched (<0.005 Ω cm wafers). b,c) TEM microscopy images of the porous nanowire from which the selected area electron diffraction (SAED, panel (b) inset) pattern was obtained. The diffraction pattern indicates the nanowire is single crystalline. Scale bars are 10 μm, 200 nm, and 50 nm for (a), (b), and (c), respectively. Adapted with permission.[101] Copyright 2009, ACS.

subjected to $HF/AgNO_3$ solution due to less band bending at the highly doped Si/solution interface compared to the lightly doped Si. Therefore, more holes were available for diffusion to Si regions without metal coverage.

7. Template-Based Metal-Assisted Chemical Etching

Controlled fabrication of Si and Si-based nanostructures is essential for the application of Si nanostructures. Metal-assisted chemical etching of Si introduced in the above section allows fabrication of Si nanowires or pores with a controlled doping level and additionally a partially a controlled orientation. However, the question of the control of the position and the diameter of nanowires remains to be solved. On the basis of the simple phenomenon of metal-assisted chemical etching, in which the Si substrate under a noble metal coverage is etched much faster than Si without noble metal coverage, Huang et al. developed a simple but versatile method to fabricate highly ordered Si nanowires, enabling control of the diameter and length of nanowire, as well as the density of nanowire arrays.[76] In principle, this approach allows control of the doping type, doping level, crystallographic orientation, and the orientation of Si nanowire relative to the Si substrate. On the basis of this method, several approaches[21,22,77,78,94,102,103] have been developed to fabricate Si nanowire arrays with various diameters, Si nanowires with sub-10 nm diameter, vertically aligned non-(100) Si nanowire arrays relative to the substrate, as well as SiGe superlattice nanowire arrays. Meanwhile, other ordered Si nanostructures including nanopillar arrays and pore arrays have successfully been fabricated.[75,104] In this section, the details of controllable fabrication of Si nanostructures is introduced.

7.1. Nanosphere Lithography Method

The key point in controlled fabrication of Si nanostructures is the deposition of a noble metal film containing position- and size-defined pores, which determine the position and size of the remaining structures after etching (Figure 6i,j). The approach of Huang et al.[76] started from self-assembly of a monolayer of a PS sphere array on the Si substrate. Subsequently, size reduction of the PS spheres was achieved by a RIE process, transferring the close-packed PS spheres into non-close-packed ones. In the next step, a noble metal film was deposited by thermal evaporation onto the Si substrate with the non-close-packed PS sphere as a mask. This process resulted in a continuous layer of noble metal with an ordered array of pores. The diameter of the pores was determined by the remaining diameter of the RIE-etched PS spheres. The Si substrate covered with the continuous film with pores, denoted as mesh hereafter, was etched in an etchant containing HF and H_2O_2. During the etching, the noble metal mesh sank vertically into the Si substrate. The unetched Si protruded from the etched surroundings on the mesh, exhibiting itself as a Si nanowire array. **Figure 14a** shows the scheme of nanosphere-lithography-based metal-assisted chemical etching and Figure 14b shows a typical SEM image of Si nanowire arrays obtained by this method, respectively.

It is revealed by SEM characterization that the average diameter of Si nanowires matches very well that of the remaining PS spheres. Using recently developed techniques in nanosphere lithography, spheres of PS or other polymers with diameters ranging from 200 nm to several micrometers are easy to assemble into highly ordered array structures on a wafer scale. Meanwhile, the mature etching processes in the semiconductor industry allow precise reduction of sphere diameter via a RIE process. Therefore, the nanosphere lithography method enables control of the diameter of Si nanowires in a wide range, from around 50 nm to several micrometers. The length of Si nanowires varies linearly with the etching time, allowing easy control of their length. The upper parts of nanowires may be bent and stuck together if the Si nanowires have a relatively large aspect ratio (ratio of length to diameter) and a high area density, and then the nanowires tend to form bundles of nanowires. The formation of bundles can be attributed to surface tension forces exerted on the nanowires during the drying of the sample,[105] which is a common phenomenon for drying of long nanowire arrays from the solvent and can be avoided with super-critical CO_2 drying.[78,106]

It has been demonstrated that Si nanowires with an aspect ratio larger than 30 could be obtained. Higher aspect ratios may be achieved simply by further increasing the etching time. The Si nanowires exhibited a slightly tapered shape. The lateral etching rate, deduced from the difference between the diameter at the bottom and top of nanowires, was typically less than 6 nm per min, while the vertical etching rate was larger than 360 nm per min (**Figure 15a**). The lateral etching can be attributed to shape evolution of the Ag mesh (Section 3.4) and/or diffusion of holes from the etching front to the side wall of Si nanowires (Section 4.2). The crystallinity of nanowires generated by metal-assisted chemical etching has been investigated by high-resolution (HR)-TEM (Figure 15). Different parts of a 3 μm long Si nanowire stored under ambient atmosphere for more than 2 months exhibited different surface features. The bottom part of the Si nanowire (close to the substrate) had an atomic-level flat (or smooth) surface covered by a layer of amorphous SiO_x with a thickness of less than 2 nm (Figure 15b). The surface of the middle part of the Si nanowire became rougher and the thickness of SiO_x increases to ca. 5 nm (Figure 15c). The top part of Si nanowire showed a very rough surface covered with an even thicker SiO_x film (≈8 nm, Figure 15d). From the bottom to the top part of a Si nanowire, the time that the side wall of Si nanowire was exposed to the HF/H_2O_2 solution and experienced the non-metal-assisted etching increases. The different exposure times were most likely responsible for the different surface roughnesses of the Si nanowire along its length. Although the surface was rough at its top, the nanowire itself showed the perfect lattice structure of a Si crystal without any observable defects, which was in contrast to some cases of Si nanowires etched by RIE.[16]

A similar approach to fabricate Si nanowires by combining metal-assisted chemical etching and nanosphere lithography was reported by Peng et al.[94] The authors used SiO_2 spheres as a mask. Prior to the deposition of metal, the SiO_2 spheres were annealed and etched in HF solution, resulting in a non-close-packed array. Subsequently, metal deposition and chemical etching were conducted to produce Si nanowire arrays.[94]

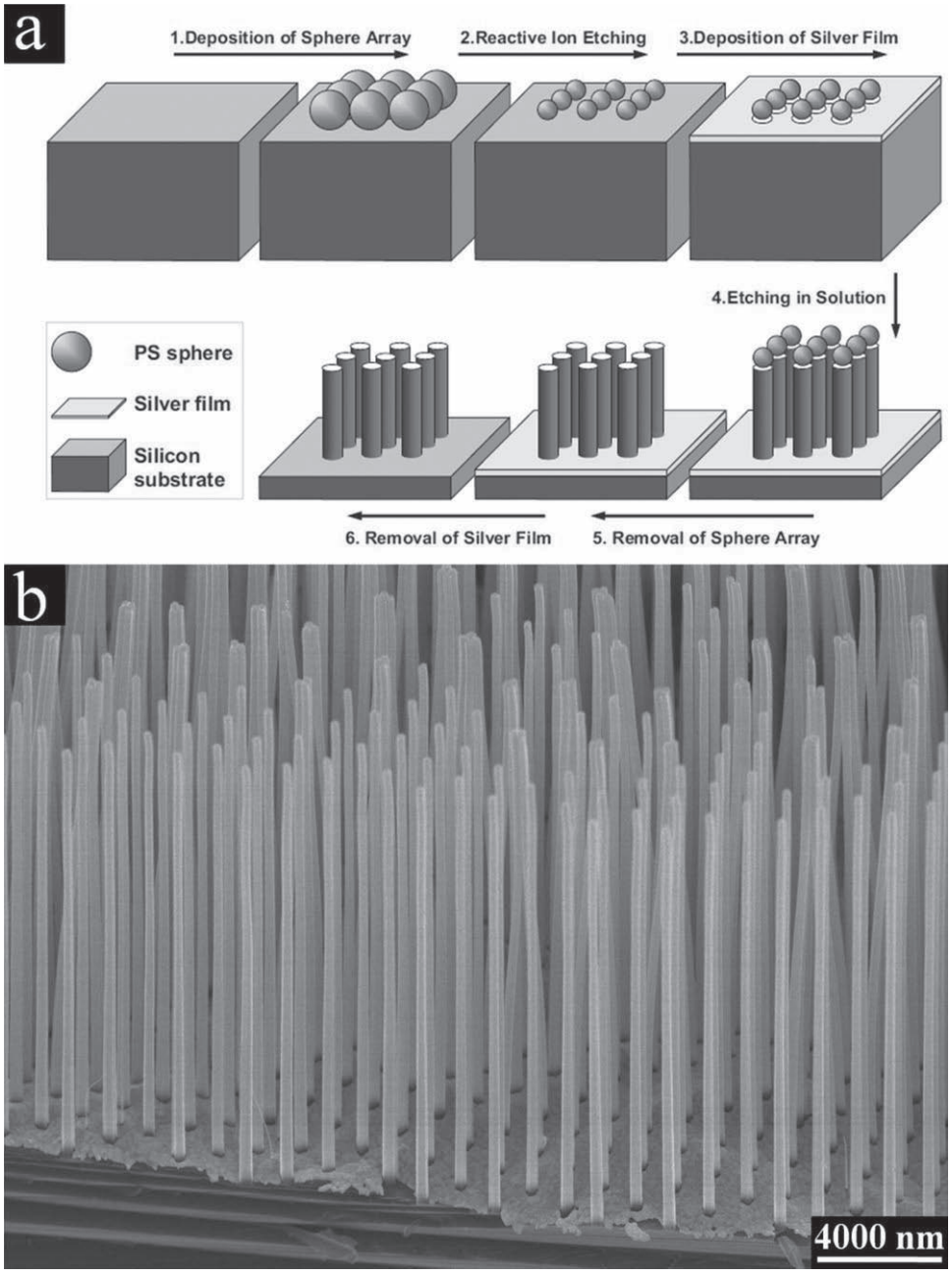

Figure 14. a) Scheme showing the processes in a method combining nanosphere lithography and metal-assisted chemical etching. Adapted with permission.[76] Copyright 2007, Wiley-VCH. b) A typical bird's-eye-view SEM image of Si nanowire arrays fabricated by the method combining nanosphere lithography and metal-assisted chemical etching.

7.2. AAO Mask Method

In practice, it is difficult to assemble polymer spheres with diameters less than ca. 200 nm into a highly ordered monolayer array. In order to fabricate Si nanowires with diameters less than 20 nm, the mask must be obtained by reducing the diameter of the polymer spheres of much larger diameter. This process usually leads to an irregular shape for the remaining polymer and is therefore not appropriate for the fabrication of Si nanowires with a well-defined circular cross-section. Furthermore, it is difficult to successfully pattern a noble metal film with arrays of discrete holes if the typical thickness of the noble metal film is comparable to the height of the size-reduced polymer spheres. For these reasons the nanosphere lithography method is usually limited to Si nanowires with diameters larger than 50 nm.

Anodic aluminum oxide (AAO) can be conveniently fabricated by the anodization of aluminum, which is characterized by a thin Al_2O_3 foil containing pores of diameters ranging from 10 to 350 nm with a density ranging from 5×10^8 pores

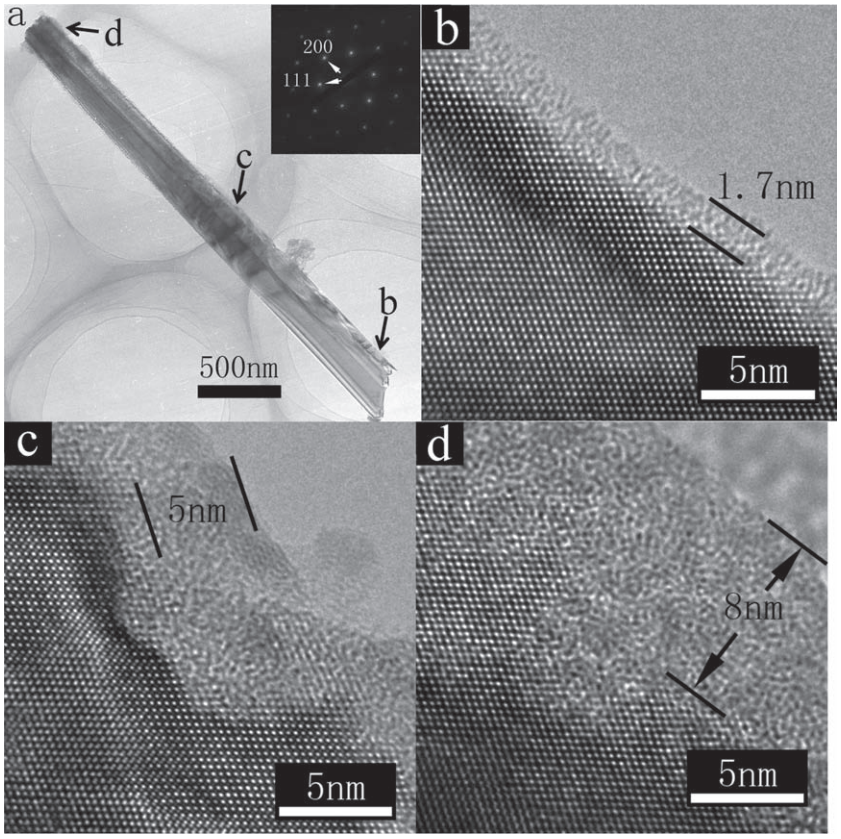

Figure 15. a) TEM image of a Si nanowire fabricated using the method combining nanosphere lithography and metal-assisted chemical etching. The inset shows the selected area electron diffraction pattern of the Si nanowire. b–d) High-resolution TEM images corresponding to the regions (b–d) that are marked with arrows in panel (a).

per cm^2 to 3×10^{10} pores per cm^2.[107,108] Huang et al. developed a method utilizing ultrathin AAO membranes as a mask to pattern a noble metal mesh, which enabled etching of a Si substrate into nanowires with diameters less than 10 nm.[77] First, an ultrathin AAO membrane (thickness ≈300 nm, pore diameter ≈20 nm) was placed on a Si substrate via a solution-based transfer process. Subsequently, RIE was performed to pattern the AAO membrane covered Si substrate in an SF_6/O_2 plasma. The hexagonal pattern of the AAO membrane was transferred onto the underlying Si substrate with a high degree of fidelity. After the removal of the AAO membrane by an acid treatment and drying of the patterned Si substrate with N_2 flux, a thin layer of silver or gold was deposited onto the patterned Si substrate. The deposited metal was characterized by a film with holes on the surface of the Si substrate, as well as isolated particles at the bottom of the RIE-etched pits in the Si substrate. By etching the metal-covered Si substrate in an etchant containing HF and H_2O_2, the substrate was transformed into Si nanowires. The size of holes in the metal mesh was determined by the size of the etch pits on the Si substrate (the size of pores in the AAO membrane) and the thickness of the metal mesh. Due to a closure effect,[109] progressive shrinkage of the aperture size in the metal mesh occurs as the deposition of metal proceeds. That is, the diameter of the holes in the metal mesh decreases with increasing mesh thickness. Based on this approach, Si nanowires with an average diameter ranging from 15 nm to 8 nm were successfully fabricated by varying the thickness of the deposited metal. HR-TEM characterization confirmed that sub-10-nm-diameter Si nanowires with high crystalline quality and smooth surface were obtained.[77]

In the approach described above, a RIE treatment was employed to pattern the Si substrate prior to the deposition of the noble metal layer. Huang et al. modified this approach, resulting in a new method that avoided RIE, so that the overall process could be finished in a chemical lab.[21] In the new method (**Figure 16a**), an ultrathin AAO membrane, with a thickness less than 100 nm, was placed on a Si substrate, as in the previous approach. The PS layer, which was utilized to protect the AAO membrane during the transfer of the AAO membrane onto the Si substrate, was removed by heating the Si substrate at 400 °C in air (step 1, Figure 16a). Next, a layer of Ag was deposited onto the AAO-covered Si substrate via sputtering. Ag formed a mesh on the AAO membrane (step 2, Figure 16a), similar to the mesh on the surface of the patterned Si substrate in the previous approach. The Ag-mesh/AAO/Si substrate was etched in the etchant (step 3, Figure 16a). At the initial stage of etching, the AAO membrane was dissolved by the HF in the etchant. Thereby, the Ag mesh initially covering the AAO membrane was transferred into direct contact with the Si substrate. The Si substrate, covered with a metal mesh, was then etched and Si nanowires were formed. Similar to the previously described approach, the thickness of the metal mesh affects the final

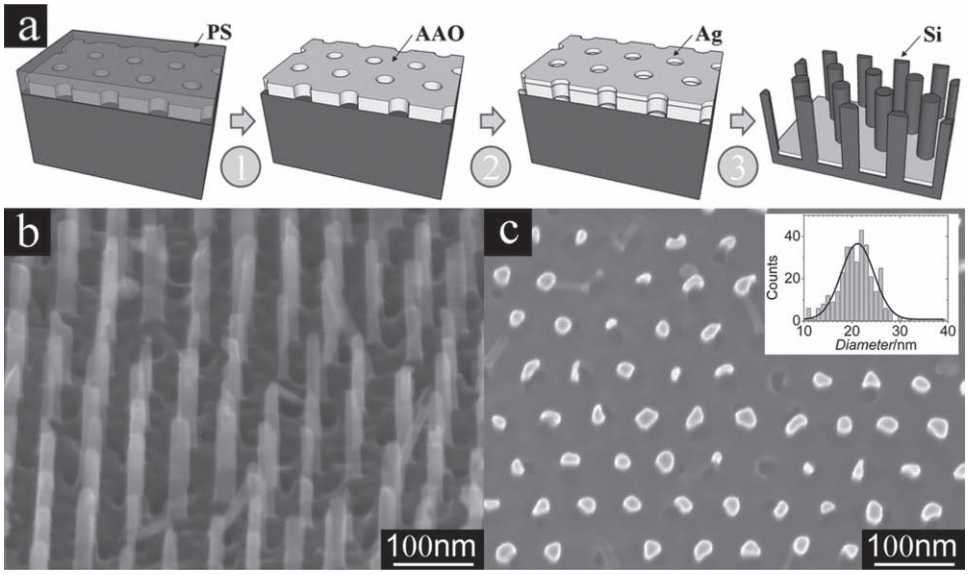

Figure 16. a) Scheme showing the fabrication process of a method combining an AAO mask and metal-assisted chemical etching. b) Bird's eye view and c) plan-view SEM images of vertical [110] Si nanowires array on a (110) substrate. Inset in (c) shows the diameter distribution of the [110] Si nanowires. Adapted with permission.[21] Copyright 2009, ACS.

diameter of the Si nanowires. Based on this method, large area arrays of vertically aligned (110) Si nanowires relative to the substrate could be obtained with diameters in the range of 20 nm (Figure 16b,c). Details on how the preferred anisotropic <100> etching can be avoided were already discussed in Section 6.1.

At this point, a comment on the etching behavior of the isolated particles located at the bottom of the Si pores or AAO pores in the two above-mentioned approaches is appropriate. Experimentally the etching rates are different for the metal mesh and the isolated metal particles in the two cases and usually metal particles can be found on the top of some Si nanowires. Although the diameter of the Si nanowire is smaller than $2W_{sc}$ here, the relatively slow etching at the top of the Si nanowire should not be attributed to the $2W_{sc}$ rule, which would deplete the small diameter nanowire in case of anodic HF etching of Si[98] because in metal-assisted chemical etching holes are injected directly from the noble metal to the Si (Section 2.3). A possible reason might be the different barrier height between the Si/mesh contact and the Si/particle contact. It has been revealed by simulation[88] and experiment[110] that the Schottky barrier height of Si/metal contact increases as the size of contact decreases. The higher barrier leads to slower hole injection and hence lower etching rate. Since metal particles do not always move along the vertical direction, it cannot be excluded that the particles are lost from the top of the Si nanowire by non-vertical etching and only very slow non-metal-assisted etching occurs at the top of Si nanowires. Finally, it should be mentioned that the silicon in the RIE-etched pores might show a thin defective region that might prevent or at least severely hinder metal-assisted etching.

In addition to Si nanowires, SiGe nanowires can also be fabricated using this method. Geyer et al.[103] applied the method to a substrate consisting of 40 periods of alternating Si (8.4 Å) and Ge (2.1 Å) layers (**Figure 17a**) and obtained sub-20-nm-diameter nanowires containing a Si/Ge superlattice (Figure 17b). HR-TEM investigations showed a smooth surface of the Si/Ge superlattice nanowires (Figure 17c) and a high-quality crystalline structure (Figure 17d). After etching, the Si/Ge superlattice in an etched nanowire maintained the atomic structure and an abrupt Si/Ge interface exactly as in the unetched substrate. This result confirmed that the metal-assisted chemical etching did not disturb the crystallographic structure of the Si/Ge superlattices. The smooth surface of the Si/Ge superlattice nanowires suggests that the etching behavior of the Si layer and Ge layer is nearly identical. No "under-cut" was found at the interface between the Si and Ge layers. The successful etching of Si/Ge superlattice substrate into Si/Ge nanowires might be associated with the fine period of the multilayer and low Ge concentration (≈20%) because Heck et al. found that poly-SiGe with Ge concentrations below 80% have no observable etching rate after 40 h, although poly-Ge was etched in H_2O_2 at a rate of 400 nm per min.[111]

7.3. Interference Lithography Method

Defects and domain structures are inevitable in the array of nanosphere and self-ordered AAO masks. Therefore, it is very difficult to fabricate defect-free Si nanowire arrays using AAO masks (unless the AAO masks were seeded via long-range-ordered nanoimprint stamps obtained by electron beam lithography, which will be the subject of a future publication). The self-ordered AAO array structure is limited to hexagonal structures and usually the cross-sectional shape of Si nanowires is circular. In order to obtain Si nanowires with different array structures, different cross-sectional shape, and perfect ordering, Choi et al. defined the mask using interference lithography (IL) and applied the mask to the

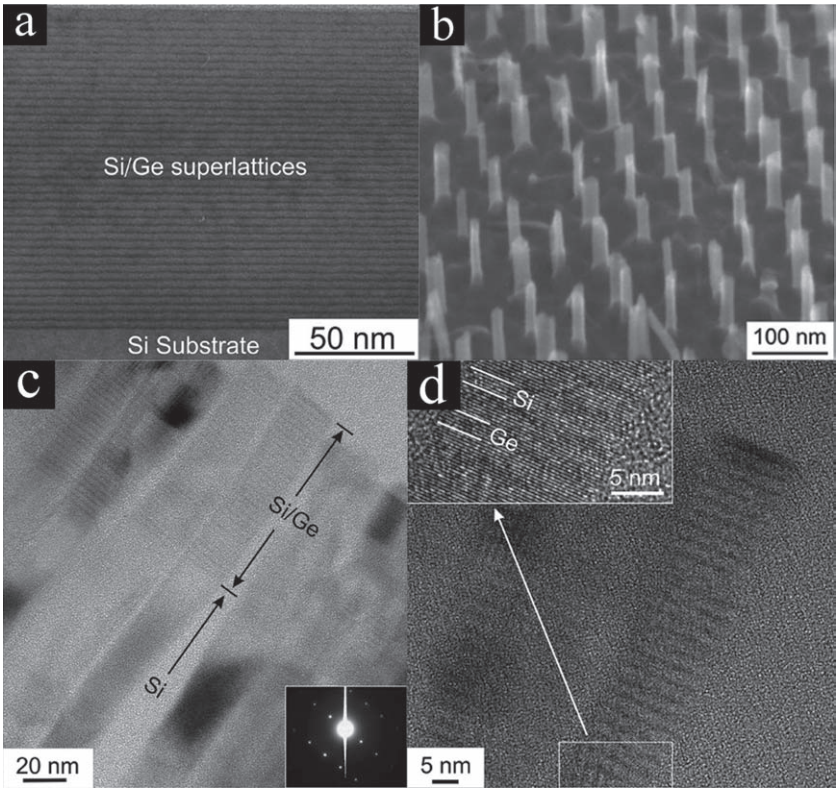

Figure 17. a) Cross-sectional TEM image of a layer of Si/Ge supperlattice (40 periods) on Si substrate. b) Bird's eye view SEM image of Si/Ge nanowires fabricated by combining an AAO mask and metal-assisted chemical etching. c) TEM image indicates clearly the Si and Ge heterostructures of a 18-nm-diameter Si/Ge nanowire. Sharp transitions between the Si and the Si/Ge layers are visible. The inset is the selected area electron diffraction image showing the single crystallinity of the Si/Ge nanowires. d) Cross-sectional high-resolution TEM image of two Si/Ge nanowires. The magnified TEM lattice image in the inset demonstrates the single crystallinity of the Si/Ge nanowires. Adapted with permission.[103] Copyright 2009, ACS.

metal-assisted chemical etching (**Figure 18**).[22] First, the Si substrate was coated by a layer of ≈400 nm thick photoresist. The cured photoresist was then exposed in a Lloyd's mirror type interference lithography setup with a 325 nm wavelength laser source. The unexposed photoresist was removed by proper developing, leaving behind the exposed photoresist on the substrate. Subsequently, oxygen plasma etching was employed to reduce the size of the exposed photoresist and to remove the residual unexposed photoresist. The substrate was then subjected to a metal (Au) deposition and metal-assisted chemical etching, resulting in a perfectly ordered Si nanowire array. By adjusting the exposure process, photoresist openings with various cross-sectional shapes, including circles, ovals, and rectangles, could be fabricated. Accordingly, Si nanowires with circular or square cross-sections or Si nanofin arrays were obtained. For a laser with a 325 nm wavelength, the density of the Si nanowire array can be tuned from 3.5×10^5 wires per mm^2 to 4×10^6 wires per mm^2. Si nanowires with a diameter of 150 nm were fabricated by this method. The approach also allows production of diperiodic structures. Recently, J. de Boor et al. have extended the ability of IL-based metal-assisted chemical etching to fabricate Si nanowire arrays with wire diameters as small as 65 nm.[23]

7.4. Block-Copolymer Mask Method

Chang et al. used block-copolymers as a mask to fabricate a metal mesh, creating high aspect ratio Si nanowires with diameters less than 20 nm.[78] A Si substrate was coated with 60-nm-thick SiO_2 by e-beam evaporation. The ordered structure of a diblock copolymer, polystyrene-block-ployferroceny ldimethylsilane (PS-*b*-PFS), on the SiO_2/Si was obtained by spin-coating and vacuum annealing (**Figure 19a**). Subsequently, the PS matrix was removed by an oxygen plasma, leaving behind PFS as dot arrays on the SiO_2/Si substrate (Figure 19b). The SiO_2 film was transferred into pillars by RIE with the PFS dots acting as a mask (Figure 19c). Gold was deposited onto the SiO2 pillar arrays by e-beam evaporation (Figure 19d). The SiO_2 pillars were removed in diluted HF solution, leaving behind a mesh on the Si substrate in which the diameter of the pores had a good fidelity to the diameter of the PFS dots (Figure 19e). Finally, ordered arrays of Si nanowires were obtained by etching the Si substrate with the Au mesh in an etchant containing HF and H_2O_2 (Figure 19f). By this approach, diameters of the Si nanowire as small as 19 nm could be realized. The spacing between the nanowires was 10 nm (corresponding approximately to a lattice constant of the nanowire array of 30 nm). Prepatterning the substrate with trenches and assembling the diblock copolymer into the trenches, the authors obtained wires-in-trench structures and stripes of Si nanowire arrays. From long-time etching, Si nanowires with an aspect ratio as high as 220 were obtained (Figure 19g).

7.5. Other Structures Based on the Nanosphere Lithography Method

By proper metal-induced etching, Si substrates can be transformed not only into pillar arrays but also into ordered pore arrays. A monolayer array of close-packed PS spheres was used as a mask to deposit a layer of a noble metal (Ag). Masked with PS spheres, Ag particles residing in interstices of the spheres formed an ordered array in a hexagonal arrangement. The Ag-loaded substrate was then etched in the etchant, resulting in a patterned structure. Etched in a solution containing HF (0.9 M) and $Fe(NO_3)_3$ (0.0675 M), Si pillars formed with each pillar located under a PS sphere.[75] The formation of a pillar under each PS sphere could be attributed to etching of Si without metal coverage in HF/$Fe(NO_3)_3$ solution, as discussed in Section 4.1.

During etching in a HF/H_2O_2 solution, pores are formed in a substrate, with the positions of the pores corresponding to the initial positions of the Ag particles. This phenomenon was also reported by Asoh et al.[104] They used a monolayer array

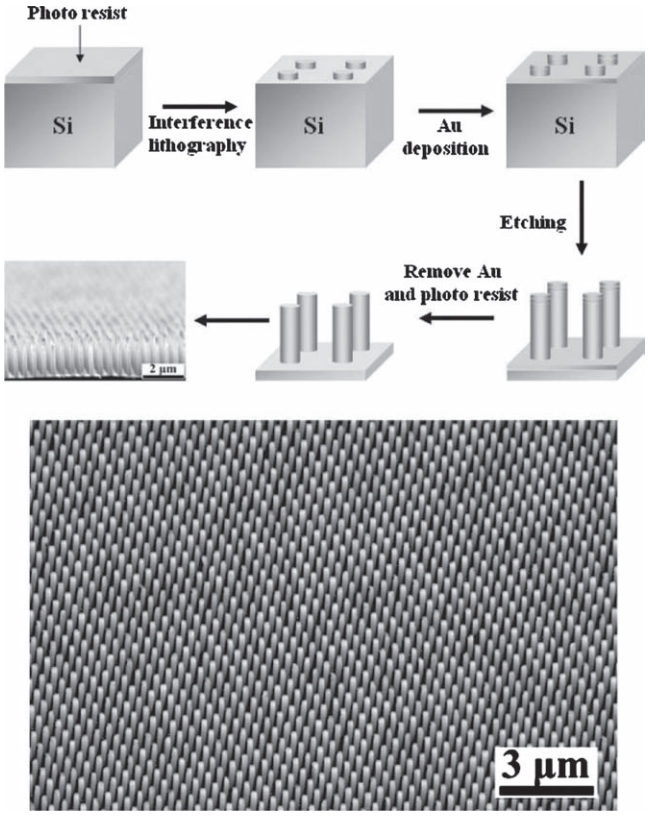

Figure 18. Scheme showing the processes involved in a method combining interference lithography and metal-assisted chemical etching and the corresponding SEM image of the resulting Si nanowires structure. Adapted with permission.[22] Copyright 2008, ACS.

of close-packed PS spheres as mask and plated the Si substrate with $AgClO_4$ and NaOH, which led to isolated Ag particles in the interstices of the PS spheres. Subsequently, the Ag-loaded Si substrate was etched in HF (5 M) and H_2O_2 (1 M), resulting in pores arranged in the form of a honeycomb lattice.

8. Metal-Assisted Chemical Etching of Other Semiconductors

Pure Ge can be etched in H_2O_2 solution.[111] Therefore, the metal-assisted etching of pure Ge substrate in HF/H_2O_2 solution has not yet been reported. In the aqueous solution of Ag^+ salt (e.g., $AgNO_3$, Ag_2SO_4, $AgClO_4$, or $Ag(CH_3CO_2)$), Ag^+ was reduced to Ag particles on the Ge substrate and the Ge under Ag particles was catalytically etched into pits (**Figure 20a**).[112] The Ge–Ge bonds acted as the reducing agent for Ag^+ ions, resulting in the reduction of Ag^+ and the oxidation of Ge into Ge^{4+}.[112] Because the resulting Ge^{4+} product, germanium oxide, is water soluble, no HF is necessary in this case to etch the Ge substrate into pits.

Metal-assisted chemical etching occurs on GaAs substrate.[113,114] In a typical experiment, Ag mesh was chemically plated onto a GaAs substrate with a monolayer array of PS sphere as a mask. Afterward, the Ag-mesh-loaded GaAs substrate was subjected to an aqueous etchant composed of HF (5 mol L^{-1}) and H_2O_2 (1 mol L^{-1}) at room temperature. An array

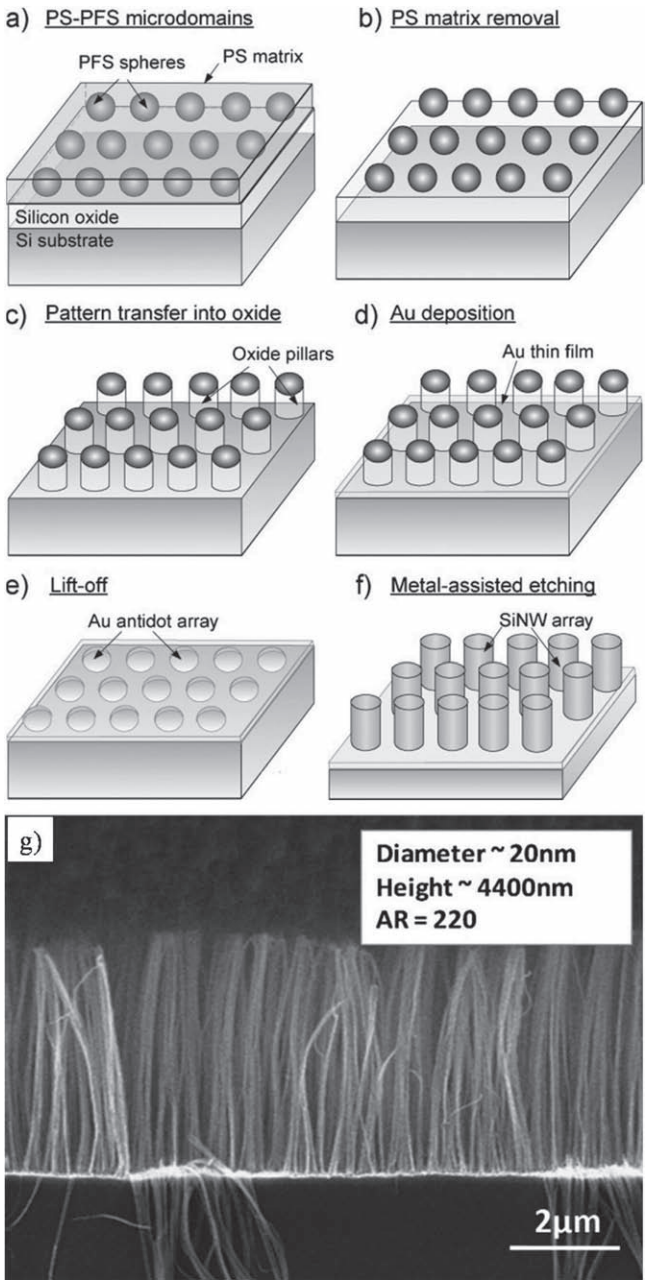

Figure 19. a–f) Scheme showing the processes involved in a method combining block-copolymer mask and metal-assisted chemical etching. g) SEM image of Si nanowire array fabricated by a method combining a block-copolymer mask and metal-assisted chemical etching. Adapted with permission.[78] Copyright 2009, Wiley-VCH.

of pillars of GaAs was obtained on the GaAs substrate after the Ag plating and sequent etching (Figure 20b).[113]

GaN can be chemically etched in HF/H_2O_2 solution with the assistance of Pt particles and the etching results in columnar pores developing mainly along the surface normal (Figure 20c).[115–117] With the same etchant and metal catalyst, the etching rate of GaN (≈45 nm per min)[115] is much slower than the etch rate of Si (>2.4 μm per min),[33] even if the etching of GaN is accelerated by UV irradiation (intensity = 30 mW cm^{-2} and wavelength,

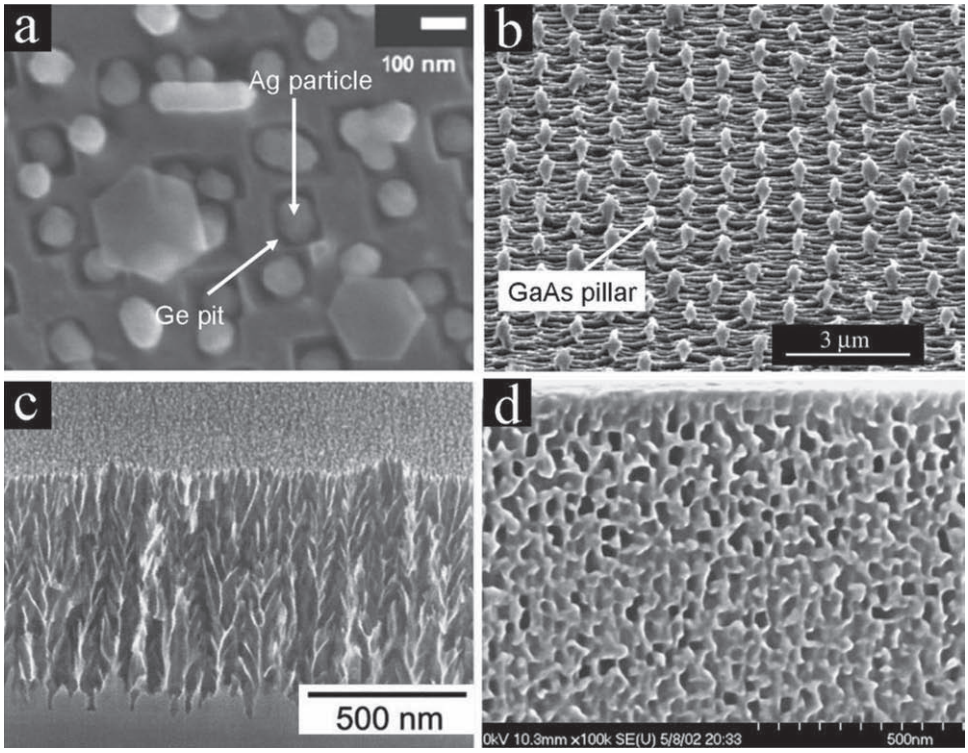

Figure 20. a) Plan-view SEM image of Ge substrate subjected to an aqueous solution of $AgNO_3$. Adapted with permission.[112] Copyright 2005, ACS. b) Bird's eye view SEM image of GaAs pillar fabricated by Ag-assisted etching of GaAs with PS sphere array as a mask. Adapted with permission.[113] Copyright 2008, Elsevier. c) Bird's eye view SEM image of pores fabricated by Pt-assisted etching oçf GaN. Adapted with permission.[115] Copyright 2002, AIP. d) Cross-sectional SEM image of interconnected pores fabricated by Pt-assisted etching of SiC. Adapted with permission.[118] Copyright 2003, Elsevier.

$\lambda < 360$ nm).[115] The slower etching rate of GaN was attributed to lower hole mobility in GaN, slower dissolution of Ga_2O_3 in HF, and a higher Schottky barrier height of Pt/GaN.[115]

A Pt-loaded SiC substrate could not be catalytically etched in HF/H_2O_2 solution, but was etched in HF solution containing more active oxidant, $K_2S_2O_8$.[118] Similarly to the etching of GaN, UV irradiation was necessary for the Pt-assisted chemical etching of SiC.[118] SiC was etched into interconnected pores (Figure 20d), but not columnar pores.[118] The reason of this specific morphology was not given.

The etching of GaAs, GaN, and SiC was explained by a simple hole injection model[113,115,118] somewhat analogous to what has been used to explain the etching of Si.[33,51] The etching behavior of elemental Ga, As, N, C, and Si would be different at the atomic scale. Meanwhile, the band gap, energy levels of valence and conduction bands, and surface states of GaAs, GaN, and SiC are different from those of Si, which might induce different hole injection processes and consequently different etching behaviors in different substrates. These differences have not yet been discussed systematically in literature.

9. Application of Structures from Metal-Assisted Chemical Etching

A porous structure is the typical morphology of Si etched from a Pt-coated substrate. Such porous silicon structures show intense photoluminescence (PL).[33] If a substrate (1–10 Ω cm) was etched with sputtered Pt (3 nm), a blue shift of the peak PL emission occurred with increasing etching time due to the generation of smaller structures, as confirmed by Raman measurements.[35]

Substrates after metal-assisted chemical etching usually look black, suggesting a prominent antireflection property of the etched structure. The hemisphere reflectance measurement of a Si substrate covered with Si nanowires, which is fabricated by etching a monocrystalline Si substrate in $AgNO_3$/HF solution or an Ag-particle-loaded Si substrate in H_2O_2/HF solution, revealed that the reflectance of the structure was less than 5% in the 300–1000 nm wavelength range.[4] Si nanowires etched from poly-crystalline Si substrates showed similar excellent antireflective properties.[4,119] Therefore, Si nanowires from metal-assisted etching are promising candidates for solar energy conversion devices. Solar cells, photochemical solar cells, and solar water splitting devices on the basis of structures from metal-assisted chemical etching (e.g., Si nanowire arrays,[4,7] inclined Si nanowire arrays,[5] Si nanowire arrays on glass,[9] core–shell p–n junction Si nanowire arrays,[6] and core-shell Si/TiO_2 junction nanowires[8]) have been demonstrated. Fang et al. reported a conversion efficiency of 11.37%,[5] which to our knowledge is the maximum efficiency among the reported solar cells built from Si nanowires by etching. Si nanowires from metal-assisted chemical etching have also been used as an anodic material in a Li^+ ion battery.[11]

A rough surface can be fabricated easily by metal-assisted chemical etching of Si. The rough structure provides a stable superhydrophobic surface on the Si substrate, with a contact angle of approximately 155°.[29,30] The superhydrophobicity can be improved in a hierarchical silicon structure etched by combining alkaline etching and metal-assisted chemical etching.[31]

Si nanowires fabricated by metal-assisted chemical etching have a rougher cylindrical surface than Si nanowires fabricated by typical VLS growth. The typical roughness of a Si nanowire by metal-assisted chemical etching is approximately 1–5 nm. The thermoelectric performance of Si nanowires appears to benefit from such rough surfaces.[26] The Seebeck coefficient and electrical resistivity of rough metal-etched Si nanowires are close to the values of bulk Si, but exhibit a 100-fold reduction in thermal conductivity, which is not found in smooth VLS-grown Si nanowires.[26]

Metal-assisted chemical etching provides a simple approach to fabricate Si nanowires and therefore is widely used as scaffold to fabricate other 1D nanostructures, e.g., SiC porous nanowires[120] or Ag-coated Si nanowires.[27,28,121] Ag-coated Si nanowires are promising substrates for molecular sensing using surface-enhanced Raman spectroscopy.[27,28]

10. Summary and Open Questions

The mechanisms and fabrication procedures of metal-assisted chemical etching were discussed here and various phenomena during the etching, including the influence of the specific noble metal, etchant, temperature, illumination, and intrinsic properties of the Si substrate on the morphological evolution of etched structures. The approaches of template-based metal-assisted chemical etching, which enable control of the diameter, length, shape, packing density, and direction of the etched Si nanowires, were also presented.

The selective etching of Si at the Si/metal interface can be tentatively attributed to hole injection during the etching process. Holes are selectively injected into the Si at the Si/noble metal interface. The injected holes can either be consumed directly at the interface in terms of etching the silicon or they can diffuse away from the interface within the Si substrate and then be consumed as part of microporous silicon formation, analogous to the process that occurs during electrochemical or stain etching. The morphological evolution during metal-assisted chemical etching (e.g., selective etching at the Si/metal interface, different catalytic activities of different metals, different morphologies of etched structures induced by etchants with different compositions, etching at off-metal areas, and partly micro- or mesoporous structures in highly doped Si substrates) are qualitatively explained in this scenario involving the injection and the diffusion of electronic holes.

The details in hole injection process have not been systematically investigated. The influence of the intrinsic properties of Si substrate (i.e., doping type and doping level), surface state of Si substrate, and the type and morphologies of the noble metal catalyst on the hole injection process remains incompletely understood. The proper explanation of some currently poorly understood phenomena, such as different etching behaviors of Si substrates with different doping type and doping level and the different etching behaviors induced by different type of metal catalysts, relies upon fully understanding of hole injection process.

During metal-assisted chemical etching of silicon substrates, the noble metal particles move into the Si substrate. The origin of the driving force of the movement of the noble metal particles is simply the preferred etching of silicon under the particles. There are clear indications for faster movement of smaller particles. Presently it is not understood in detail what determines the etching path of noble metal particles, which can be straight in specific crystallographic directions but can also be helical in certain cases. The possible role of the shape of the noble metal particle (sphere, half sphere, or disk) has not yet been investigated and resolved. Even if the initial movement directions of noble metal particles are more or less random, there is a tendency to move in the same etching direction after a sufficiently long etching time. The driving force for aligning the movement directions of adjacent particles for longer etching times, which appears to be some kind of cooperative effect, is not presently understood. Understanding, in detail, the movement of noble metal particles during the etching of Si might help to control the movement direction of noble metal particles and enable fabrication of delicate 3D Si nanostructures.

Metal-assisted chemical etching is intrinsically anisotropic. The anisotropy has been attributed to the strength of backbonds, analogous to the case of electrochemical HF etching and alkaline etching of Si. However, although the etching direction is anisotropic, the vertical etching depths for different etching directions on substrates with the same orientation or along the vertical direction on substrates with different orientations are almost the same under identical conditions. This cannot be easily understood in terms of a simple application of the backbond strength theory. As yet, a systematic study of the relationship between the etching rate, etching direction, and orientation of Si substrates is lacking.

The etched structure evolves into micro- or mesopores with increasing doping level of the Si substrate. The porous structures are most likely induced by the holes injected at the noble metal/silicon interface diffusing to the Si areas without metal coverage. A highly doped Si substrate without any metal coverage can be etched into a porous structure, while, according to the mechanism introduced in Section 2, the noble metal is necessary for the reduction of H_2O_2. There might be other unrevealed mechanisms for hole injection in highly doped Si substrates. A possible influence of the specific dopant element on the morphologies of etched structures has not been studied so far. The comprehensive understanding of etching in highly doped Si substrates will require a systematic study of the etching with different dopant elements, doping levels, etchants, and noble metals.

Metal-assisted chemical etching has been demonstrated not only on Si and Si/Ge substrate, but also on GaAs, GaN, and SiC substrates, and partially on a Ge substrate. The etching morphologies of these non-Si semiconductors have been well-characterized, whereas the details of etching mechanism are yet to be explored. Meanwhile, it is a scientifically and technically important open question to determine whether the metal-assisted chemical etching method can be extended to other semiconductors.

Even though unresolved aspects of the detailed mechanisms of metal-assisted chemical etching remain, to a high degree the etching of Si is controllable and reproducible, especially concerning the etching direction and porosity. Moreover, template-based metal-assisted chemical etching enables fabrication of Si and SiGe nanostructures with controlled diameter, shape, length, and packing density. Due to its inherent simplicity, low cost, easy process control, and reproducibility, metal-assisted chemical etching is likely to be used even more extensively as a reliable method for fabricating Si and Si/Ge nanostructures.

Acknowledgements

Z. H. and N. G. contributed equally to this article. Financial support from the German Research Foundation (STE 1127/8 –1), and the research foundation of Jiangsu University, P.R. China (09JDG043) are greatly acknowledged. The authors gratefully acknowledge the support of the interdisciplinary center of Materials Science, Martin-Luther-University Halle-Wittenberg. In particular, we thank Dr. Hartmut S. Leipner and Dr. Bodo Fuhrmann for helpful discussions. We also thank Dr. Woo Lee, Dr. Lifeng Liu, Dr. Stephan Senz, Dr. Tomohiro Shimizu, Mr. Zhang Zhang, Prof. Xuanxiong Zhang, Dr. Wilfried Erfurth, Mr. Horst Blumtritt, and Mr. Norbert Schammelt at the Max Planck Institute of Microstructure Physics (Germany) for discussions and providing original results used in this article. Prof. Gösele passed away during the preparation of the manuscript.

Received: May 14, 2010
Revised: June 25, 2010
Published online: September 21, 2010

[1] V. Schmidt, H. Riel, S. Senz, S. Karg, W. Riess, U. Gösele, *Small* **2005**, *2*, 85.
[2] J. Goldberger, A. I. Hochbaum, R. Fan, P. Yang, *Nano Lett.* **2006**, *6*, 973.
[3] B. Tian, X. Zheng, T. J. Kempa, Y. Fang, N. Yu, G. Yu, J. Huang, C. M. Lieber, *Nature* **2007**, *449*, 885.
[4] K. Q. Peng, Y. Xu, Y. Wu, Y. J. Yan, S. T. Lee, J. Zhu, *Small* **2005**, *1*, 1062.
[5] H. Fang, X. D. Li, S. Song, Y. Xu, J. Zhu, *Nanotechnology* **2008**, *19*, 255703.
[6] E. C. Garnett, P. D. Yang, *J. Am. Chem. Soc.* **2008**, *130*, 9224.
[7] K. Q. Peng, X. Wang, S. T. Lee, *Appl. Phys. Lett.* **2008**, *92*, 163103.
[8] Y. J. Hwang, A. Boukai, P. D. Yang, *Nano Lett.* **2009**, *9*, 410.
[9] V. Sivakov, G. Andra, A. Gawlik, A. Berger, J. Plentz, F. Falk, S. H. Christiansen, *Nano Lett.* **2009**, *9*, 1549.
[10] C. K. Chan, H. L. Peng, G. Liu, K. McIlwrath, X. F. Zhang, R. A. Huggins, Y. Cui, *Nat. Nanotechnol.* **2008**, *3*, 31.
[11] K. Peng, J. Jie, W. Zhang, S. T. Lee, *Appl. Phys. Lett.* **2008**, *93*, 033105.
[12] Y. Cui, Q. Wei, H. Park, C. M. Lieber, *Science* **2001**, *293*, 1289.
[13] F. Patolsky, G. Zheng, C. M. Lieber, *Nat. Protoc.* **2006**, *1*, 1711.
[14] A. K. Buin, A. Verma, A. Svizhenko, M. P. Anantram, *Nano Lett.* **2008**, *8*, 760.
[15] K. H. Hong, J. Kim, S. H. Lee, J. K. Shin, *Nano Lett.* **2008**, *8*, 1335.
[16] S. G. Cloutier, C. H. Hsu, P. A. Kossyrev, J. Xu, *Adv. Mater.* **2006**, *18*, 841.
[17] D. M. Lyons, K. M. Ryan, M. A. Morris, J. D. Holmes, *Nano Lett.* **2002**, *2*, 811.
[18] D. D. D. Ma, C. S. Lee, F. C. K. Au, S. Y. Tong, S. T. Lee, *Science* **2003**, *299*, 1874.
[19] V. Schmidt, S. Senz, U. Gosele, *Nano Lett.* **2005**, *5*, 931.
[20] Z. Huang, T. Shimizu, S. Senz, Z. Zhang, N. Geyer, U. Gösele, *J. Phys. Chem. C* **2010**, *114*, 10683.
[21] Z. P. Huang, T. Shimizu, S. Senz, Z. Zhang, X. X. Zhang, W. Lee, N. Geyer, U. Gösele, *Nano Lett.* **2009**, *9*, 2519.
[22] W. K. Choi, T. H. Liew, M. K. Dawood, *Nano Lett.* **2008**, *8*, 3799.
[23] J. de Boor, N. Geyer, J. V. Wittemann, U. Gösele, V. Schmidt, *Nanotechnology* **2010**, *21*, 095302.
[24] V. Lehmann, *J. Electrochem. Soc.* **1993**, *140*, 2836.
[25] P. Kleimann, X. Badel, J. Linnros, *Appl. Phys. Lett.* **2005**, *86*, 183108.
[26] A. I. Hochbaum, R. K. Chen, R. D. Delgado, W. J. Liang, E. C. Garnett, M. Najarian, A. Majumdar, P. D. Yang, *Nature* **2008**, *451*, 163.
[27] B. H. Zhang, H. S. Wang, L. H. Lu, K. L. Ai, G. Zhang, X. L. Cheng, *Adv. Funct. Mater.* **2008**, *18*, 2348.
[28] M. L. Zhang, C. Q. Yi, X. Fan, K. Q. Peng, N. B. Wong, M. S. Yang, R. Q. Zhang, S. T. Lee, *Appl. Phys. Lett.* **2008**, *92*, 043116.
[29] M. W. Cao, X. Y. Song, J. Zhai, J. B. Wang, Y. L. Wang, *J. Phys. Chem. B* **2006**, *110*, 13072.
[30] F. Shi, Y. Y. Song, H. Niu, X. H. Xia, Z. Q. Wang, X. Zhang, *Chem. Mater.* **2006**, *18*, 1365.
[31] Y. Xiu, L. Zhu, D. W. Hess, C. P. Wong, *Nano Lett.* **2007**, *7*, 3388.
[32] D. Dimova Malinovska, M. Sendova Vassileva, N. Tzenov, M. Kamenova, *Thin Solid Films* **1997**, *297*, 9.
[33] X. Li, P. W. Bohn, *Appl. Phys. Lett.* **2000**, *77*, 2572.
[34] K. Tsujino, M. Matsumura, *Electrochem. Solid St. Lett.* **2005**, *8*, C193.
[35] S. Chattopadhyay, X. L. Li, P. W. Bohn, *J. App. Phys.* **2002**, *91*, 6134.
[36] K. Q. Peng, H. Fang, J. J. Hu, Y. Wu, J. Zhu, Y. J. Yan, S. Lee, *Chem.–Eur. J.* **2006**, *12*, 7942.
[37] C. Y. Chen, C. S. Wu, C. J. Chou, T. J. Yen, *Adv. Mater.* **2008**, *20*, 3811.
[38] C. L. Lee, K. Tsujino, Y. Kanda, S. Ikeda, M. Matsumura, *J. Mater. Chem.* **2008**, *18*, 1015.
[39] C. Chartier, S. Bastide, C. Levy-Clement, *Electrochimica Acta* **2008**, *53*, 5509.
[40] K. Peng, A. Lu, R. Zhang, S. T. Lee, *Adv. Funct. Mater.* **2008**, *18*, 3026.
[41] M. L. Zhang, K. Q. Peng, X. Fan, J. S. Jie, R. Q. Zhang, S. T. Lee, N. B. Wong, *J. Phys. Chem. C* **2008**, *112*, 4444.
[42] T. Unagami, *J. Electrochem. Soc.* **1980**, *127*, 476.
[43] E. S. Kooij, K. Butter, J. J. Kelly, *Electrochem. Solid St. Lett.* **1999**, *2*, 178.
[44] Y. Harada, X. L. Li, P. W. Bohn, R. G. Nuzzo, *J. Am. Chem. Soc.* **2001**, *123*, 8709.
[45] S. Yae, Y. Kawamoto, H. Tanaka, N. Fukumuro, H. Matsuda, *Electrochem. Commun.* **2003**, *5*, 632.
[46] K. Q. Peng, Y. J. Yan, S. P. Gao, J. Zhu, *Adv. Funct. Mater.* **2003**, *13*, 127.
[47] T. Hadjersi, *Appl. Surf. Sci.* **2007**, *253*, 4156.
[48] K. Tsujino, M. Matsumura, *Electrochim. Acta* **2007**, *53*, 28.
[49] X. H. Xia, C. M. A. Ashruf, P. J. French, J. J. Kelly, *Chem. Mater.* **2000**, *12*, 1671.
[50] K. Q. Peng, Y. Wu, H. Fang, X. Y. Zhong, Y. Xu, J. Zhu, *Angew. Chem. Int. Ed.* **2005**, *44*, 2737.
[51] K. Q. Peng, J. J. Hu, Y. J. Yan, Y. Wu, H. Fang, Y. Xu, S. T. Lee, J. Zhu, *Adv. Funct. Mater.* **2006**, *16*, 387.
[52] H. Asoh, S. Sakamoto, S. Ono, *J. Colloid Interface Sci.* **2007**, *316*, 547.
[53] S. Ono, A. Oide, H. Asoh, *Electrochim. Acta* **2007**, *52*, 2898.
[54] D. R. Turner, *J. Electrochem. Soc.* **1960**, *107*, 810.
[55] T. Hadjersi, N. Gabouze, E. S. Kooij, A. Zinine, A. Ababou, W. Chergui, H. Cheraga, S. Belhousse, A. Djeghri, *Thin Solid Films* **2004**, *459*, 271.
[56] S. Cruz, A. Honig-dOrville, J. Muller, *J. Electrochem. Soc.* **2005**, *152*, C418.
[57] K. Tsujino, M. Matsumura, *Adv. Mater.* **2005**, *17*, 1045.
[58] Q. W. Chen, X. J. Li, Y. H. Zhang, *High Pressure Res.* **2001**, *20*, 1.
[59] M. Nahidi, K. W. Kolasinski, *J. Electrochem. Soc.* **2006**, *153*, C19.

[60] K. S. Nahm, Y. H. Seo, H. J. Lee, *J. App. Phys.* **1997**, *81*, 2418.
[61] Y. H. Seo, K. S. Nahm, K. B. Lee, *J. Electrochem. Soc.* **1993**, *140*, 1453.
[62] V. Lehmann, *Electrochemistry of Silicon: Instrumentation, Science, Materials, and Applications*, Wiley-VCH, **2002**.
[63] J. C. Huang, R. K. Sen, E. Yeager, *J. Electrochem. Soc.* **1979**, *126*, 786.
[64] S. Gottesfeld, I. D. Raistrick, S. Srinivasan, *J. Electrochem. Soc.* **1987**, *134*, 1455.
[65] Y. J. Li, R. Lenigk, X. Z. Wu, B. Gruendig, S. J. Dong, R. Renneberg, *Electroanalysis* **1998**, *10*, 671.
[66] X. H. Cai, K. Kalcher, G. Kolbl, C. Neuhold, W. Diewald, B. Ogorevc, *Electroanalysis* **1995**, *7*, 340.
[67] R. Zeis, T. Lei, K. Sieradzki, J. Snyder, J. Erlebacher, *J. Catal.* **2008**, *253*, 132.
[68] G. Flatgen, S. Wasle, M. Lubke, C. Eickes, G. Radhakrishnan, K. Doblhofer, G. Ertl, *Electrochim. Acta* **1999**, *44*, 4499.
[69] A. Hiraki, M-A. Nicolet, J. W. Mayer, *Appl. Phys. Lett.* **1971**, *18*, 178.
[70] A. Cros, J. Derrien, F. Salvan, *Surf. Sci.* **1981**, *110*, 471.
[71] T. Xie, V. Schmidt, E. Pippel, S. Senz, U. Gösele, *Small* **2008**, *4*, 64.
[72] P. Werner, C. C. Buttner, L. Schubert, G. Gerth, N. D. Zakarov, U. Gosele, *Int. J. Mater. Res.* **2007**, *98*, 1066.
[73] C. C. Buttner, N. D. Zakharov, E. Pippel, U. Gosele, P. Werner, *Semicond. Sci. Technol.* **2008**, *23*.
[74] H. Fang, Y. Wu, J. H. Zhao, J. Zhu, *Nanotechnology* **2006**, *17*, 3768.
[75] Z. P. Huang, Y. Wu, H. Fang, N. Deng, T. L. Ren, J. Zhu, *Nanotechnology* **2006**, *17*, 1476.
[76] Z. P. Huang, H. Fang, J. Zhu, *Adv. Mater.* **2007**, *19*, 744.
[77] Z. P. Huang, X. X. Zhang, M. Reiche, L. F. Liu, W. Lee, T. Shimizu, S. Senz, U. Gosele, *Nano Lett.* **2008**, *8*, 3046.
[78] S. W. Chang, V. P. Chuang, S. T. Boles, C. A. Ross, C. V. Thompson, *Adv. Funct. Mater.* **2009**, *19*, 2495.
[79] S. Chattopadhyay, P. W. Bohn, *J. App. Phys.* **2004**, *96*, 6888.
[80] Y. H. Ogata, K. Kobayashi, M. Motoyama, *Curr. Opin. Solid State Mater. Sci.* **2006**, *10*, 163.
[81] K. Q. Peng, J. Zhu, *J. Electroanal. Chem.* **2003**, *558*, 35.
[82] Y. Y. Song, Z. D. Gao, J. J. Kelly, X. H. Xia, *Electrochem. Solid St.* **2005**, *8*, C148.
[83] T. Qiu, X. L. Wu, G. G. Siu, P. K. Chu, *J. Electron. Mater.* **2006**, *35*, 1879.
[84] K. Q. Peng, J. Zhu, *Electrochim. Acta* **2004**, *49*, 2563.
[85] T. Qiu, X. L. Wu, Y. F. Mei, G. J. Wan, P. K. Chu, G. G. Siu, *J. Cryst. Growth* **2005**, *277*, 143.
[86] T. Selvaraju, R. Ramaraj, *J. Appl. Electrochem.* **2009**, *39*, 321.
[87] S. You, M. Choi, *J. Aerosol Sci.* **2007**, *38*, 1140.
[88] J. P. Sullivan, R. T. Tung, M. R. Pinto, W. R. Graham, *J. Appl. Phys.* **1991**, *70*, 7403.
[89] K. Q. Peng, Z. P. Huang, J. Zhu, *Adv. Mater.* **2004**, *16*, 73.
[90] K. Q. Peng, Y. J. Yan, S. P. Gao, J. Zhu, *Adv. Mater.* **2002**, *14*, 1164.
[91] L. Koker, A. Wellner, P. A. J. Sherratt, R. Neuendorf, K. W. Kolasinski, *J. Phys. Chem. B* **2002**, *106*, 4424.
[92] J. Frayret, A. Castetbon, G. Trouve, M. Potin-Gautier, *Chem. Phys. Lett.* **2006**, *427*, 356.
[93] S. L. Cheng, C. H. Chung, H. C. Lee, *J. Electrochem. Soc.* **2008**, *155*, D711.
[94] K. Q. Peng, M. L. Zhang, A. J. Lu, N. B. Wong, R. Q. Zhang, S. T. Lee, *Appl. Phys. Lett.* **2007**, *90*, 163123.
[95] Y. M. Yang, P. K. Chu, Z. W. Wu, S. H. Pu, T. F. Hung, K. F. Huo, G. X. Qian, W. J. Zhang, X. L. Wu, *Appl. Surf. Sci.* **2008**, *254*, 5648.
[96] H. Morinaga, M. Suyama, T. Ohmi, *J. Electrochem. Soc.* **1994**, *141*, 2834.
[97] X. H. Xia, C. M. A. Ashruf, P. J. French, J. Rappich, J. J. Kelly, *J. Phys. Chem. B* **2001**, *105*, 5722.
[98] X. G. Zhang, *Electrochemistry of Silicon and Its Oxide.*, Kluwer Academic/Plenum Publisher, New York **2001**.
[99] P. M. M. C. Bressers, J. J. Kelly, J. G. E. Gardeniers, M. Elwenspoek, *J. Electrochem. Soc.* **1996**, *143*, 1744.
[100] M. Schade, N. Geyer, B. Fuhrmann, F. Heyroth, H. S. Leipner, *Appl. Phys. A: Mater. Sci. Process.* **2009**, *95*, 325.
[101] A. I. Hochbaum, D. Gargas, Y. J. Hwang, P. Yang, *Nano Lett.* **2009**, *9*, 3550.
[102] X. Wang, K. L. Pey, W. K. Choi, C. K. F. Ho, E. Fitzgerald, D. Antoniadis, *Electrochem. Solid St. Lett.* **2009**, *12*, K37.
[103] N. Geyer, Z. Huang, B. Fuhrmann, S. Grimm, M. Reiche, T.-K. Nguyen-Duc, J. de Boor, H. S. Leipner, P. Werner, U. Gösele, *Nano Lett.* **2009**, *9*, 3106.
[104] H. Asoh, F. Arai, S. Ono, *Electrochem. Commun.* **2007**, *9*, 535.
[105] K. Zhu, T. B. Vinzant, N. R. Neale, A. J. Frank, *Nano Lett.* **2007**, *7*, 3739.
[106] Y. Q. Liang, C. G. Zhen, D. C. Zou, D. S. Xu, *J. Am. Chem. Soc.* **2004**, *126*, 16338.
[107] H. Masuda, K. Fukuda, *Science* **1995**, *268*, 1466.
[108] A. P. Li, F. Muller, A. Birner, K. Nielsch, U. Gosele, *J. App. Phys.* **1998**, *84*, 6023.
[109] Y. Lei, W. K. Chim, *Chem. Mater.* **2005**, *17*, 580.
[110] R. C. Rossi, M. X. Tan, N. S. Lewis, *Appl. Phys. Lett.* **2000**, *77*, 2698.
[111] J. M. Heck, C. G. Keller, A. E. Franke, L. Muller, T.-J. King, R. T. Howe, "High Aspect Ratio Polysilicon-Germanium Microstructures", presented at *Proc. 10th Int. Conf. on Solid-State Sensors and Actuators*, Sendai, Japan **1999**.
[112] M. Aizawa, A. M. Cooper, M. Malac, J. M. Buriak, *Nano Lett.* **2005**, *5*, 815.
[113] Y. Yasukawa, H. Asoh, S. Ono, *Electrochem. Commun.* **2008**, *10*, 757.
[114] Y. Yasukawa, H. Asoh, S. Ono, *J. Electrochem. Soc.* **2009**, *156*, H777.
[115] X. L. Li, K. Y.-W., P. W. Bohn, I. Adesida, *Appl. Phys. Lett.* **2002**, *80*, 980.
[116] D. J. Diaz, T. L. Williamson, I. Adesida, P. W. Bohn, R. J. Molnar, *J. Vac. Sci. Technol., B* **2002**, *20*, 2375.
[117] D. J. Diaz, T. L. Williamson, I. Adesida, P. W. Bohn, R. J. Molnar, *J. Appl. Phys.* **2003**, *94*, 7526.
[118] T. L. Rittenhouse, P. W. Bohn, I. Adesida, *Solid State Commun* **2003**, *126*, 245.
[119] K. Tsujino, M. Matsumura, Y. Nishimoto, *Sol. Energy Mater. Sol. Cells* **2006**, *90*, 100.
[120] Y. J. Yang, G. W. Meng, X. Y. Liu, L. D. Zhang, Z. Hu, C. Y. He, Y. M. Hu, *J. Phys. Chem. C* **2008**, *112*, 20126.
[121] C. X. Zhang, P. Chen, J. Liu, Y. H. Zhang, W. Shen, H. L. Xu, Y. Tang, *Chem. Commun.* **2008**, 3290.